UNIVERSITY OF OKLAHOMA

GRADUATE COLLEGE

EXPERIMENTAL INVESTIGATION OF THE EFFECTS OF ROTATIONAL SPEED AND WEIGHT ON BIT ON DRILLSTRING VIBRATIONS, TORQUE AND RATE OF PENETRATION

A THESIS

SUBMITTED TO THE GRADUATE FACULTY

in partial fulfillment of the requirements for the

Degree of

MASTER OF SCIENCE

By

VIMLESH BAVADIYA
Norman, Oklahoma
2017

EXPERIMENTAL INVESTIGATION OF THE EFFECTS OF ROTATIONAL SPEED AND WEIGHT ON BIT ON DRILLSTRING VIBRATIONS, TORQUE AND RATE OF PENETRATION

A THESIS APPROVED FOR THE
MEWBOURNE SCHOOL OF PETROLEUM AND GEOLOGICAL ENGINEERING

BY

_____
Dr. Ramadan Ahmed, Chair

_____
Dr. Catalin Teodoriu

_____
Dr. Saeed Salehi

To my Family, Teachers, Friends and The Cosmic Power.

Acknowledgements

I would like to express my sincere gratitude to Dr. Ramadan Ahmed for his continuous academic guidance and unwavering support. His immense knowledge and insight have greatly helped in designing the rig for the Drillbotics competiton and winning it. I felt honored for being entrusted with the leadership of Drillbotics Team for two consecutive years. He was very patient and always motivating, and he trusted the decisions I made. He has always believed in me and helped me realize my potential.

I would like to thank Dr. Catalin Teodoriu for his critical suggestions to improve the rig design. I am also grateful to Dr. Saeed Salehi for taking interest in my research and providing valuable recommendations as a thesis committee member.

I am thankful for the SPE DSATS team for organizing the Drillbotics competition. I am grateful to Mewbourne Oil Company for providing the funding. I heartily appreciate all the help I received from my teammates Mohammad Aljubran, John Kibe, Stephen Christy, Henry Le, Kyle Gustafson, Zeeneb Alsaihati, Abdulhameed Alsousy and Adaku Akabogu.

Special thanks to Jeff McCaskill and Joel Young for their machining and technical support whenever we were stuck in a jam. I am extremely grateful to Harsh and Anuj for sticking with me through thick and thin.

Without the love and support of my family and friends the journey would not have been a joyous success. I will forever be indebted to them for the sacrifices they have made for me.

Table of Contents

List of Tables

List of Figures

Abstract

Drillstring vibrations namely torsional, axial and lateral vibrations are the primary source for downhole tool failure and reduction in rate of penetration. Bottom hole assembly, bit design, wellbore hydraulics, bit-rock interaction, drillstring-borehole interaction and drilling parameters are the factors which affect vibrations. Weight on bit and rotational speed are the influential parameters, which can be changed in real time by the driller to affect vibrations. Hence, it has been a topic of interest for researchers to find an optimum range of drilling parameters to drill efficiently.

A fully automated drilling rig was constructed for Drillbotics competition with sensors to measure rotational speed, WOB, displacement, vibration velocity, drill pipe deflection, torque, and other operational parameters. A data acquisition module was installed to collect data and control equipment using Excel based VBA program.

Two sets of experiments were performed on rock samples with different strength to study the effects of rotational speed and WOB on vibrations, torque and ROP. Axial vibration increased when drillstring was rotated at its natural frequency resulting in improvement in ROP. Coupling of axial vibration and lateral vibrations were observed at high rotational speed and WOB.

Using existing model, parametric study was carried out to analyze the impacts of bit strength to rock strength ratio, bit constant and intrinsic specific energy on torque. Results of the analysis reveal that bit constant is an important parameter to accurately predict the torque.

CHAPTER 1. INTRODUCTION

1.1 Overview

With increase in oil and gas demand, different unconventional sources are being explored utilizing new drilling and exploration techniques. Drilling is becoming a complex process. Oil and gas wells are drilled using a rotary bit attached to tubulars that are connected to each other to form a long string (drillstring), which transfers axial force and torque (Fig. 1.1). The drillstring is divided into two categories, drill pipes and Bottom Hole Assembly (BHA). The BHA often consists of drill collars, heavy weight drill pipes, Measurement While Drilling (MWD) tools and other tools such as stabilizers, reamers, bent sub and mud motor.

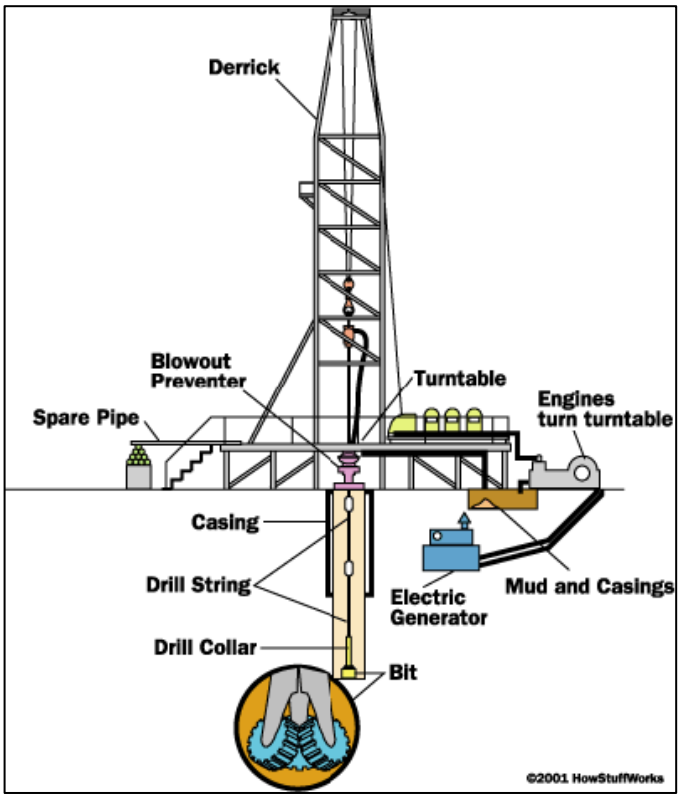

Figure 1.1: Drilling rig setup (Freudenrich and Strickland 2001)

Drillstring vibration is one of the major detrimental factors that reduce drilling efficiency. Unpredictable geology along with factors like bit-rock interaction, drillstring-borehole interaction and hydraulics make the vibration problem very challenging. Borehole deviation, borehole instability, BHA and tool damage are common factors resulting in non-productive time due to vibration.

Some of the oil and gas sources are too deep or too complex to be explored; however, with advanced technological development in drilling such as extended reach, multilateral and horizontal wells, along with advanced fluid hydraulics and completion technologies, it is now possible to produce unconventional oil and gas economically. Oil industry is extremely volatile and hence the price of oil governs the use of new and expensive technologies. During downturn cycles, the industry moves towards cost cutting by optimizing operations. MWD tools and mud motors are now used even in vertical wells to improve performance. Drilling efficiency is improved by increasing rate of penetration and decreasing non-productive time. Vibration cannot be completely eliminated from the process. Nevertheless, understanding how different factors influence vibrations will help to reduce them by using downhole vibration dampening tools or surface controllers.

1.2 Problem Statement

With the increase in need for energy, deeper and complex reservoirs are taped in to fulfill the need and keep it sustainable. Deeper and complex reservoir incurs high cost due to costly technological advances used to reach the target. To drill efficiently technological advancement has been made in fluid hydraulics, bit design, tubular

strength, steering of bit, MWD tools, sensors and mud motors. MWD services are expensive and are prone to get damaged frequently.

The three modes of vibration are torsional, lateral and axial, which have specific types called stick-slip, whirl and bit bounce, respectively. These vibrations affect the drilling process differently and have self-induced coupling effects which makes them difficult to understand and predict. Vibration during the drilling process causes damage to the downhole sensors, destroys bit cutters and BHA components, induces borehole instability and reduces rate of penetration. It is imperative to eliminate or minimize the vibration to reduce non-productive time and cost, making deep reservoirs economically viable to produce.

Optimization of control parameters such as WOB and rotational speed is important to increase efficiency. A long drillstring does not allow the vibration to reach surface and hence the impact of change in surface parameter on BHA vibration is difficult to predict. It is necessary to evaluate the drilling performance at different WOB and rotational speed.

Drilling industry is gradually moving toward automation and a process cannot be safely and efficiently automated unless it is completely understood and properly modeled. Knowing the output of the process at a specific input helps engineers design the system constraints for automation.

Several researchers have developed models and carried out lab scaled experiments along with field data comparison (Finnie and Bailey 1960, Dykstra et al. 1994, Jogi et al. 2002, Bailey et al. 2008, Patil and Teodoriu 2013b). Most of the lab scaled setup do not actually drill rock but only imitate the process. This study is carried out to obtain insights

from experimental standpoint about factors affecting drillstring vibrations, torque and ROP.

1.3 Objectives of the Research

To mitigate vibrations, it is important to understand the factors affecting vibrations. Many analytical models have been proposed to better understand vibrations. This study focusses on the controllable parameters during drilling to investigate their effect on the BHA vibrations. Hence, main objectives of this study are:

- To understand how drilling parameters such as WOB and rotational speed affect BHA vibrations and ROP.
- To evaluate performance of existing torque models.
- To characterize formations based on intrinsic specific energy calculated from the experimental drilling data.
- To identify operational parameters, which are harmful for the drillstring.
- To analyze the parameters which affect the bit torque.

1.4 Methodology

Research carried out by other investigators (Berlioz et al. 1996, Mihajlovic et al. 2007, Esmaeili et al. 2012, Tingey 2013) has been studied to get a better understanding of how drilling parameters affect vibration and what to expect from experiments. Analytical models characterizing different vibration modes along with coupling effects have been investigated.

Automated drilling rig constructed for Drillbotics competition was used to investigate how rotational speed and WOB affects drillstring vibration, torque and ROP. The control code makes the drilling process automatic, where controlled parameters such

as WOB and rotational speed were kept constant. Once theoretical constraints on the drillstring were calculated, test runs were conducted to find the operational constraints on WOB and rotational speed to create a test matrix. Experiments were conducted varying rotational speed and weight on bit for two different rock types (soft and hard sandstone). Measurements are analyzed and compared with results of previous studies. Analytical torque model by Detournay and Defourny (1992) has been validated using the experimental data.

Sensitivity analysis has been carried out to find major factors affecting the prediction of torque. Using experimental data and data from analytical model, intrinsic specific energy of the rock is estimated. Comparing the axial vibration data obtained from the experiments with the Vibration Severity Standards, optimum drilling parameters can be selected.

1.5 Thesis Outline

This document is divided into 5 chapters. Chapter 2 discusses the literature review on types of vibrations. It also includes discussion on previous studies and analytical torque model. Experimental setup and detailed rig components are described in Chapter 3. The chapter also includes experimental procedure and sensor calibration method. Chapter 4 presents data analysis and discussions of the result. Conclusion of the study and recommendations for future work are provided in Chapter 5. Appendix A contains supplemental figures and data.

CHAPTER 2. BACKGROUND STUDY

2.1 Drillstring Vibration

When an entity oscillates around its equilibrium point, the entity is said to be in vibration. In most of the cases vibrations are undesirable, as they cause harm to the system. When force or energy is imparted to a system, vibrations occur. In absence of external excitation, the vibrations are called free vibrations. If the system is in a state of free vibrations, then it oscillates with natural frequencies, which are dependent on the system characteristics. In the presence of external excitation, vibrations experienced by the system are called forced vibrations. Vibrations become increasingly large and are most damaging when the excitation frequency is close to one of the natural frequencies. This phenomenon is called resonance. When there is energy dissipation from the system in terms of heat, sound, friction or any other method, the resulting vibrations are called damped vibrations.

The drillstring assembly is a long and slender system prone to excessive vibration due to the various forces acting on it. Primary forces acting on the BHA are torque due to rotation, axial forces due to gravity, WOB and lateral forces due to bending of the long pipe and hitting the walls of the borehole. Operational stability zone for a drag bit is shown in Fig. 2.1. With an increase in WOB, there is an increase in occurrence of stick-slip and with an increase in rotational speed there is an increase in bit whirl.

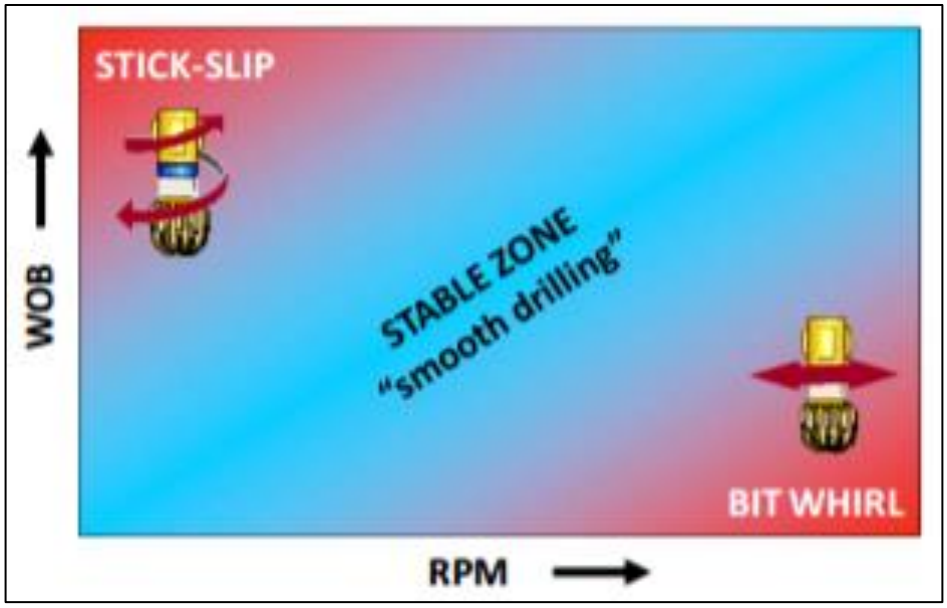

Figure 2.1: Stable zone for a PDC bit (Jain et al. 2011)

Drillstring vibrations are categorized based on the forces acting on it, which are torsional, axial and lateral forces. These forces correspond to the three modes of vibration: 1) Torsional vibrations, 2) Lateral vibrations and 3) Axial vibrations. The frequency response of these vibrations lie in the range of 0 - 0.5 Hz for torsional vibrations, 0.6 - 75 Hz for lateral vibrations and 0.8 - 42 Hz for axial vibrations as can be observed from Fig. 2.2.

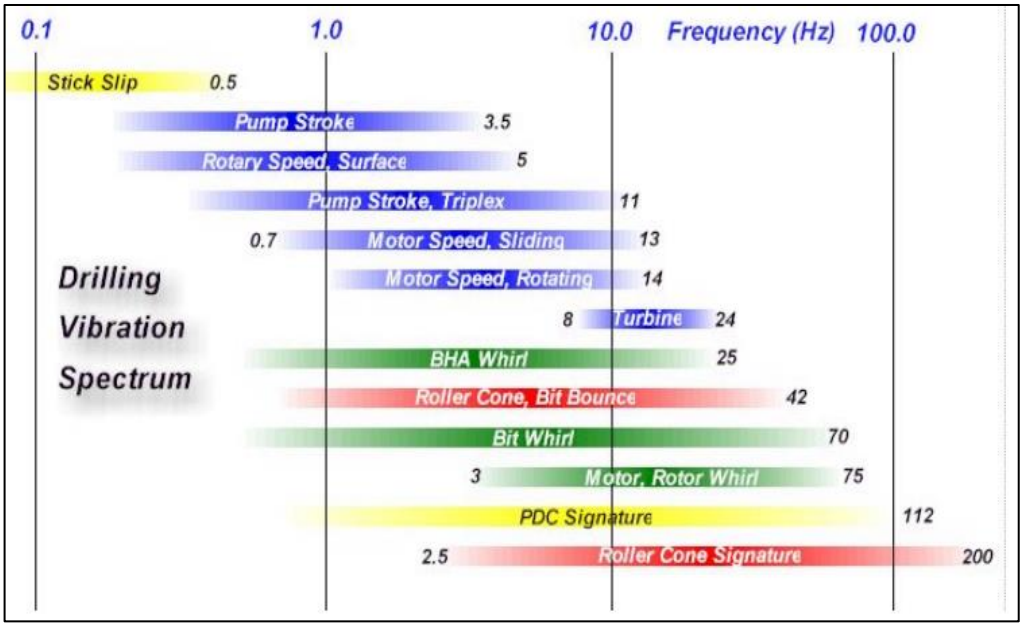

Figure 2.2: Drilling vibration frequency spectrum (Macpherson et al. 2001)

2.1.1 Torsional Vibration

Drillstring is rotated from the surface to provide torque or shear force to cut the rock. The rotary speed at the bottom is not the same as provided at the surface by the top drive or the rotary table. Due to non-linear relationship between torque and rotary speed at the bit, fluctuation in downhole speed occur (Jansen and Steen 1995). This fluctuation is self-excited and is known as Stick-slip. Flexibility and length of the drillstring exacerbates the non-uniform oscillatory behavior as it has a capacity to store energy. The storage of energy causes large variation between surface and downhole rotary speeds (Brett 1992). Stick slip induces fatigue in drillstring and increases bit damage. It is more likely to develop in a drag bit than roller cone bit.

The most common method of modelling a drillstring to study torsional vibrations is to assume the drillstring as a torsional pendulum. Modifications are made to the

pendulum model for individual cases. Halsey et al. (1986) derived equations for individual sections of drillstring and developed a computer program to calculate torsional resonance frequencies. Lin and Wang (1991) developed a dry-friction based model and carried out parametric studies to observe the effect of viscous damping, rotational speed and natural frequency on torsional vibration. Stick slip was also analyzed based on bit-rock interaction by Challamel et al. (2000). Patil and Teodoriu (2013a) formulated a mathematical model and investigated the influences of rotational speed, WOB, stiffness and inertia of the drillstring on stick-slip oscillations.

2.1.2 Lateral Vibration

Lateral vibration of drillstring occurs when center of mass of the drillstring does not coincide with the axis of rotation. As the drillstring rotates, a centrifugal force develops at the center of mass which causes it to bend and excites lateral vibrations called whirl (Vandiver et al. 1990). Whirl is classified in two forms, forward and backward. Backward whirl is the most destructive of all the vibrations. Mass imbalance also intensifies the lateral vibrations (Dykstra et al. 1996). BHA interacts with the borehole and generate shocks which damage its components and bottomhole sensors (Mitchell and Allen 1987).

Numerical studies were carried out by Jansen (1991) to analyze influence of drilling fluid, stabilizer clearance and stabilizer friction on lateral vibration. Chen and Geradin (1995) developed a transfer matrix to study the dynamics of BHA at various rotational speeds, WOBs and drilling fluids. Gulyaev et al. (2006) derived constitutive equations to analyze buckling mode of drillstring under compressive forces.

2.1.3 Axial Vibration

Irregular motion of drillstring along its longitudinal axis is called axial vibration. It causes bit bounce and significant damage to the bit and BHA components (Tucker and Wang 2000). The frequency of axial vibrations in a roller cone bit is three times that of a PDC bit (Chin 2014).

A field study (Finnie and Bailey 1960) was carried out for the first time to measure axial and torsional motions. Charts were developed based on trial and error method for easy graphical solution of natural frequencies (Bailey and Finnie 1960). Later, assuming only intermittent bit-tooth contact as the external excitation force, axial vibration was analyzed (Paslay and Bogy 1963). Dareing and Livesay (1968) studied the effects of friction damping and critical rotational speed on axial vibration. Length of drill collars has a significant impact on vibration and shock absorbers are effective in minimizing it (Dearing 1984). Dareing (1985) studied how vibration helps in improving drilling efficiency by optimizing available power at the bit. Recently, axial vibrations in air and gas drilling were studied (Li and Guo 2007). The study suggested that bit-displacement models predicted resonance speeds better than bit force models.

Developing a fully coupled vibration model, which includes all influential parameters is quite complex. Baumgart (2000) derived nonlinear differential equations accounting for axial, lateral and rotational motion of the pipe along with flow rate and pressure of drilling fluid while excluding bending related motions. Later, a fully coupled model, which accounts for bit-rock and drillstring-borehole interactions was developed (Christoforou and Yigit 2001) to design a control strategy to mitigate stick-slip

oscillations. Recently, Khulief and Al-Naser (2005) developed a dynamic drillstring model with 12 degree of freedom using FEM method along with Lagrangian approach.

2.2 Mechanistic Bit Torque Model

It is important to describe bit-rock interaction as bit oscillations generated from the interaction and coupling mechanisms increase axial and lateral vibrations. Swenson et al. (1981) built a finite element model to analyze fracture mechanism due to single PDC cutter using maximum tensile strength and shear stress criterion. Based on static balance of forces acting on a single PDC cutter, an analytic model (Wojtanowicz and Kuru 1993) was later developed. The model uses three separate equations for ROP, torque and bit life. The model depends on empirical bit constants; as a result, it cannot be used for experimental bit design.

Drag bit model developed by Detournay and Defourny (1992) have been widely used to predict downhole torque. The model provides a relationship between WOB, torque, rotational speed and ROP. It is based on the single cutter model. Two bit-rock interaction processes (cutting and frictional contact) are considered in the model. When formulating the single cutter model, the vertical velocity is assumed zero and the forces acting on the bit are considered proportional to the area of cut. A symmetric cut is assumed where the horizontal force orthogonal to the direction of cut is zero. It is assumed that the cutting forces act only on the cutter face and the frictional forces act only on the wear flat. With the assumption that intrinsic specific energy is independent of the depth of cut, the model can only be used for depth of cut between 0.1 - 2 mm which is generally the case for PDC cutters.

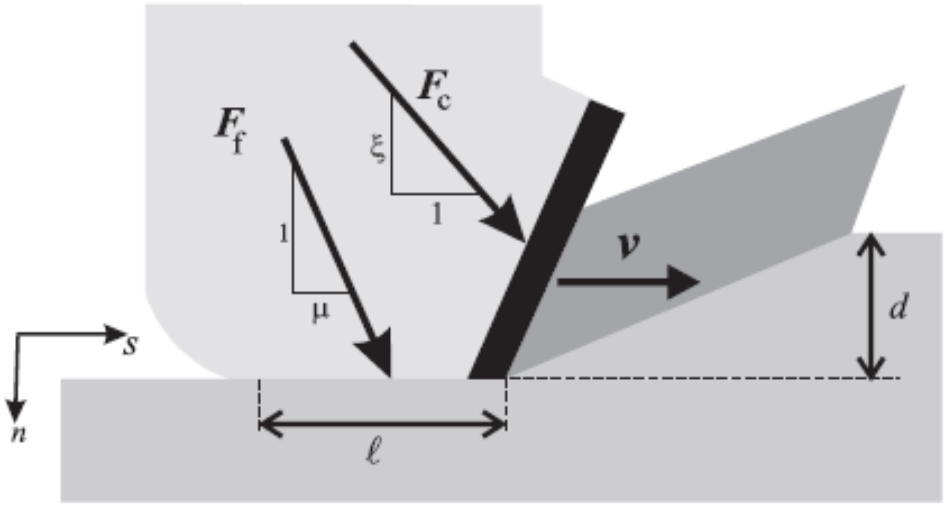

Figure 2.3: Diagram of forces acting on a blunt cutter (Richard et al. 2007)

According to Detournay and Defourny model, WOB and torque are decomposed into cutting and frictional components.

$$T = T_c + T_f \tag{2.1}$$

$$W = W_c + W_f \tag{2.2}$$

where W is WOB, T is torque and subscripts c and f correspond to the cutting and frictional processes. The force on the cutter face is assumed proportional to the cross-sectional area (A) of the groove traced by the cutter, which makes the cutting process independent of the cutter and bit geometry. Therefore, the cutting torque and WOB can be estimated using the following equations:

$$T_c = \frac{1}{2}\epsilon\delta a^2 \tag{2.3}$$

$$W_c = \zeta\epsilon\delta a \tag{2.4}$$

where a is bit radius in inches, ϵ is intrinsic specific energy of the rock in psi, ζ is ratio of drillstring strength to rock strength and δ is the depth of cut in inches estimated by the following equation:

$$\delta = \frac{2\pi v}{\omega} \tag{2.5}$$

where ω is rotational speed and *v* is ROP in in/hr. The bit constant is used to account for the frictional components of torque and WOB.

$$\gamma = \frac{2T_f}{\mu a W_f} \tag{2.6}$$

where μ is coefficient of friction. Combining Eqns. (2.3) to (2.6) and rearranging, the following formula for torque can be developed.

$$T = \frac{a}{2}[(1 - \mu\gamma\zeta)\epsilon\delta a + \mu\gamma W] \tag{2.7}$$

Torque predictions obtained from Eqn. (2.7) have been compared with the actual experimental torque. The comparison is presented in the Section 4.2. The drilling response model (Eqn. 2.7) is also expressed in terms of drilling specific energy E and drilling strength S as defined below.

$$\mathrm{E} = \frac{2T}{a^2\delta} \tag{2.8}$$

$$\mathrm{S} = \frac{W}{a\delta} \tag{2.9}$$

Dividing Eqn. (2.7) by aδ, following relation can be obtained between E and S.

$$\mathrm{E} = E_o + \mu\gamma\mathrm{S} \tag{2.10}$$

where

$$E_o = (1 - \beta)\epsilon \text{ and } \beta = \gamma\mu\zeta \tag{2.11}$$

Bit response model along with E-S diagram (Fig. 2.10) helps understand drilling process and provides a framework to interpret field data. With accurate data of WOB, torque, rotational speed and ROP, different drilled lithology could be distinguished. The value of β in Fig. 2.4 is less than 1, which is a general case for bits involving frictional

component of cutting force. Linear regression was applied to the data set provided in Fig. 2.5 and intrinsic specific energy of the rock was estimated (230 MPa) and drilling strength to rock strength ratio was 0.69, under the assumption that bit constant is one. Similar analysis was carried in this study, which is presented in Section 4.2.

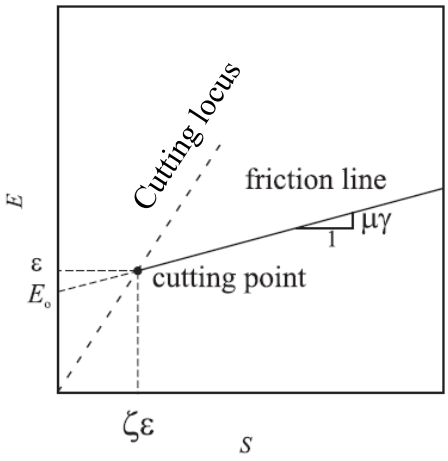

Figure 2.4: Conceptual E-S diagram

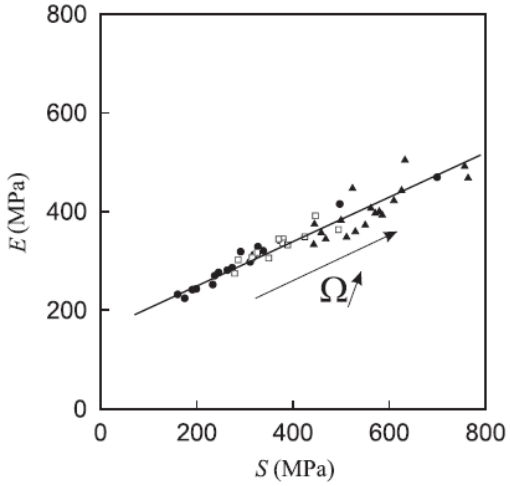

Figure 2.5: E-S diagram by Black et al. 1986 (after Richard et al. 2007)

2.3 Previous Studies

To study vibrations and its effects several test rigs have been developed by academia and industry. These rigs can be divided into subgroups of full scaled test rigs, laboratory setups and scaled systems. Glowka (1989) performed single cutter tests with varying amount of wear on different rocks (Berea Sandstone, Tennesse Marble and Sierra White Granite). Bit diameter and cutter density were changed to observe interacting and non-interacting cuts. The results showed that the cutter penetrating force is independent of the diameter of cutter. Taking the results into consideration it can be observed that Eqn. (2.4) does not contain any bit constant term. When tests were carried out with water jet assistance a decrease (10 - 15 % at 2000 psi nozzle pressure drop and 50 - 65 % at

4500 psi) in cutting force was observed. No significant change in stresses was observed at 80 psi.

Finnie and Bailey (1960) were one of the initial researchers to experimentally study the drillstring vibrations. A field study was carried out to observe vibrations in terms of frequencies and amplitudes. Berlioz et al. (1996) studied lateral vibration and its coupling with axial and torsional vibration. They built an experimental setup where a rod can be periodically excited with axial and torsional forces (Fig. 2.6). Results of numerical analysis and experiments showed that natural lateral frequencies decrease with compression force. Higher density and viscosity of fluids also reduce the lateral frequency of the rod.

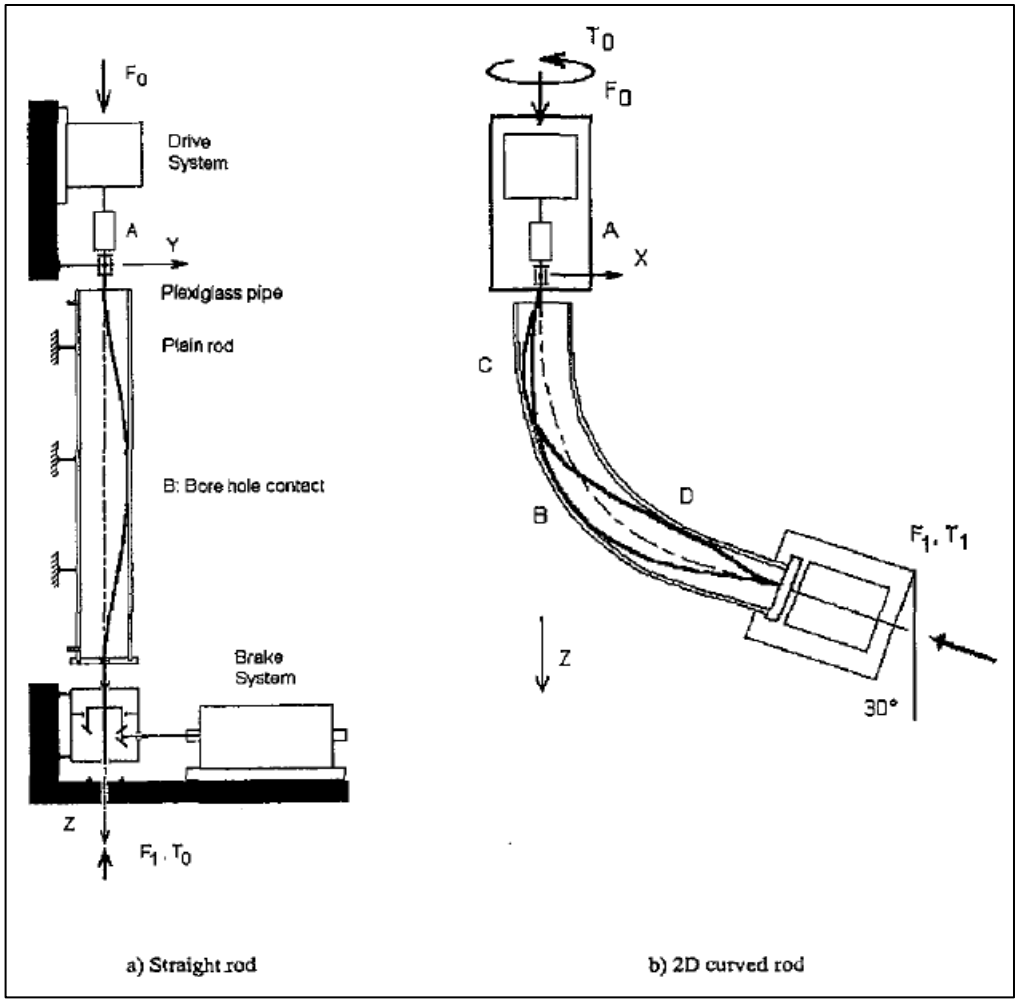

Figure 2.6: Schematic of experimental setup (Berlioz et al. 1996)

Melakhessou et al. (2003) developed an experimental setup similar to Berlioz et al. (1996) by adding a small disk at the center of the rod to simulate a tool joint (Fig. 2.7). The study examined the effects of interaction of tool-joint and drillstring with the wellbore. Numerical simulations were carried out and found that the initial string position is important for dynamic analysis of the drillstring. Another setup similar to Berlioz was constructed by Khulief and Al-Sulaiman (2009) with a shaker at the bottom of the brake to excite axial vibrations. The rig could simulate stick-slip, drillstring /wellbore contact and fluid interaction. This setup was used to validate dynamic drillstring models derived

using Lagrange approach which included torsional-bending coupling and axial-bending non-linear coupling.

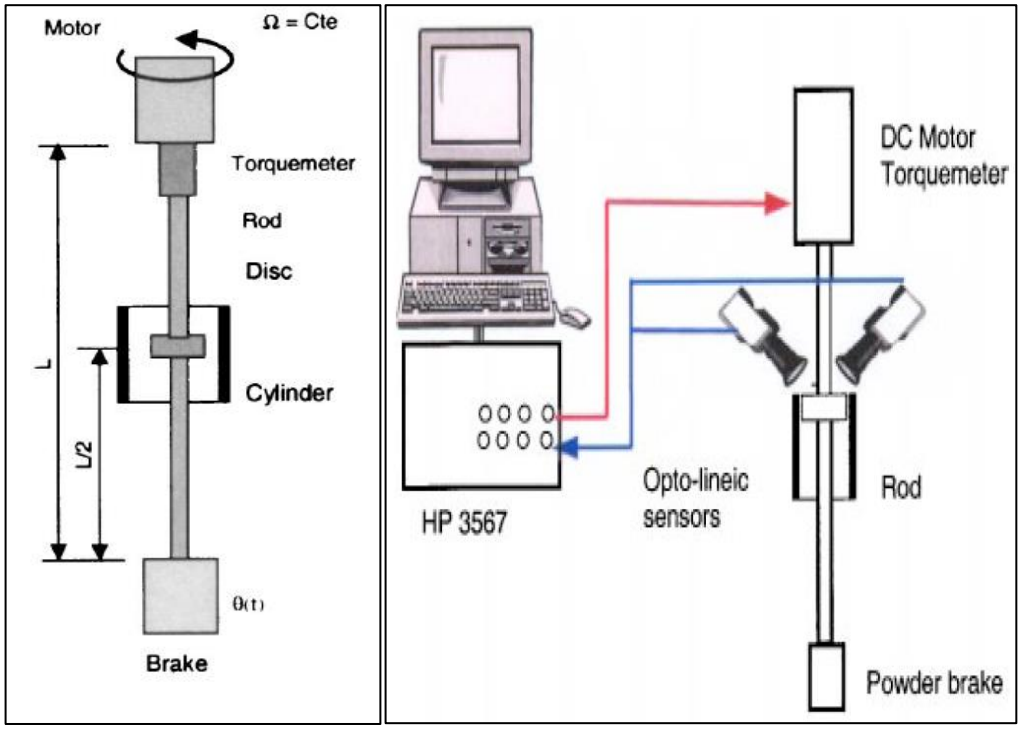

Figure 2.7: Laboratory setup diagram (Melakhessou et al. 2003)

Mihajlovic et al. (2007) studied interaction between friction induced torsional vibration and lateral vibration. A test setup was constructed with flexible string between 2 discs (Fig. 2.8). The brake on the lower disc provides friction similar to drilling action without the cutting part. Through experiments and models, they confirmed that torsional vibration decrease in presence of lateral vibration. This phenomenon was attributed to the dissipation of kinetic energy from the bit rock interaction to the lateral vibrations and not getting stored as potential energy in the slim string to cause stick-slip.

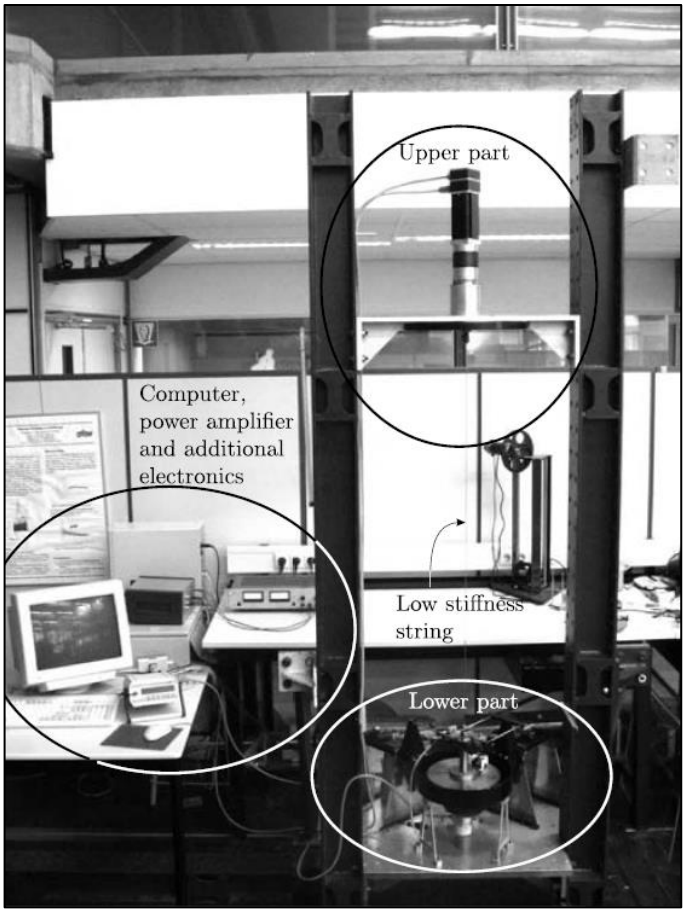

Figure 2.8: Lab-scale experimental setup (Mihajlovic et al. 2007)

A model based control approach was used by Raymond et al. (2008) to reproduce dynamic characteristics of a drillstring, removing the limitation of separate fixtures. The scope of the research was limited to axial vibration only. Initially simulation of drillstring was carried out using a mechanical analog control setup which was then modified to a model based control setup (Fig. 2.9). Actuators were used to apply the numerically predicted displacement at the interface of bit and BHA to simulate deep downhole conditions.

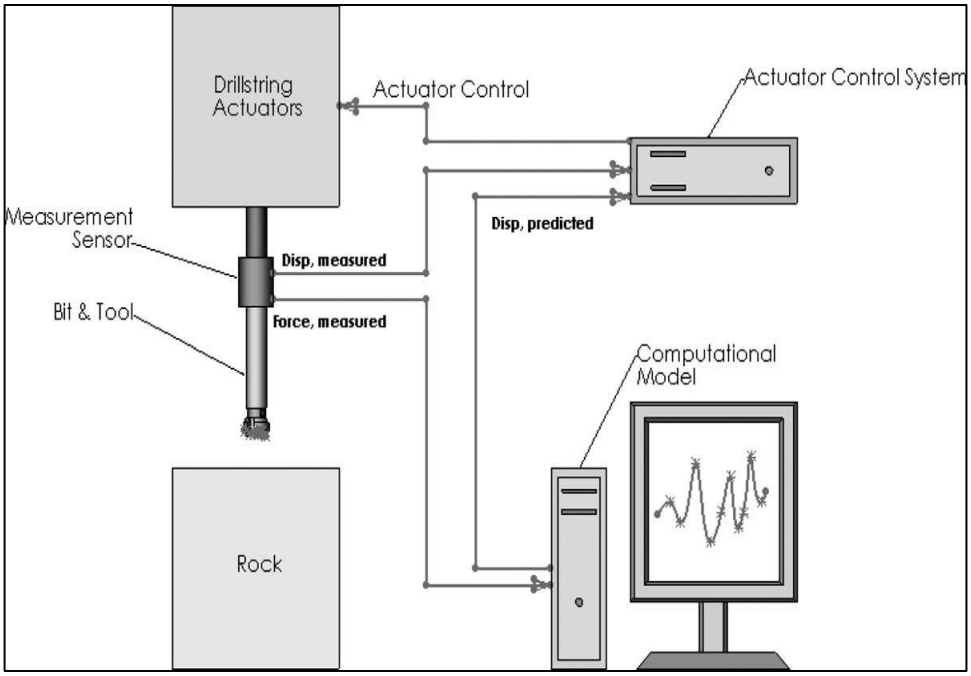

Figure 2.9: Model based control setup (Raymond et al. 2008)

Wilson (2013) and Tingey (2015) constructed a bit force measurement testing rig to measure vibrations in BHA and validate bit-force interface law developed from the results of Wilson (Fig. 2.10). Initial set of experimental results performed by Tingey at low rotational speed were compared with analytical results in which torque varied from 10 to 53 % and WOB varied from 395 to 570 %.

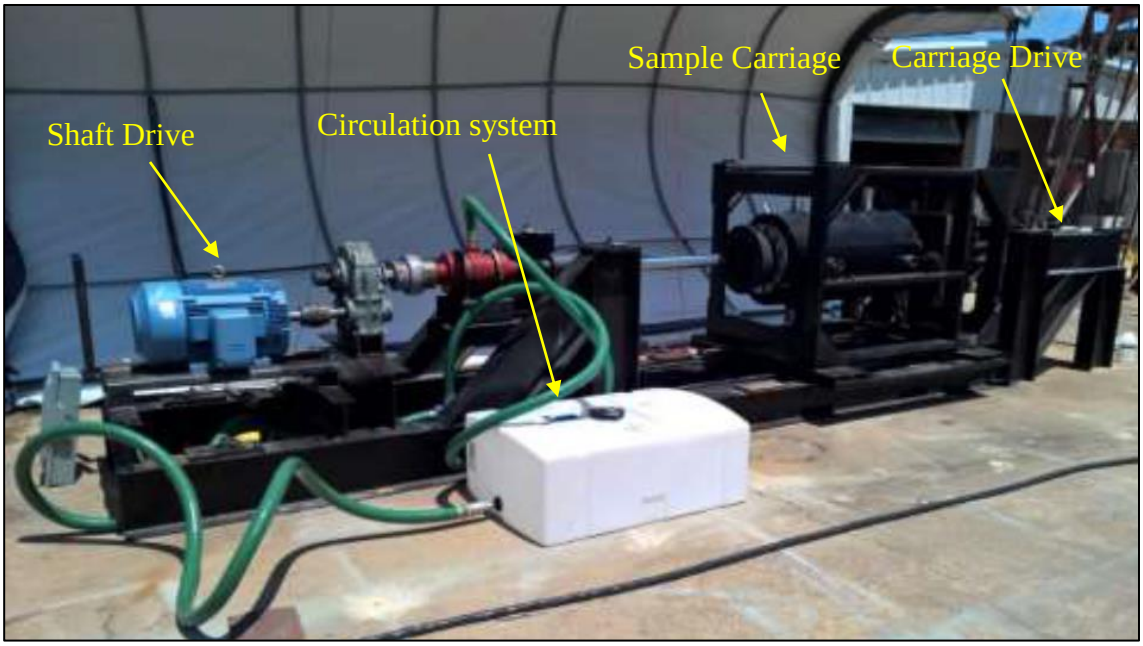

Figure 2.10: Experimental setup (Tingey 2015)

Halsey et al (1986) developed a test rig to analyze the torsional resonance frequencies. A test rig was designed by Lu et al. (2009) to reproduce stick-slip vibration and use D-OSKIL mechanism to control and minimize the torsional vibration. Franca (2010) built a lab scale setup to study the drilling response of roller cone bits. Using averaged parameters over a revolution of the bit, predictions of an analytical model was validated with experimental measurements without the need of precise description of bit geometry. Laboratory and field experiments were carried out by Forster et al. (2010) to test their Asymmetric Vibration Damping tools, which were successful in damping lateral and torsional vibrations. Forster (2011) demonstrated that axial excitations help in reducing stick-slip oscillations. An experimental rig was designed by Cheng et al. (2011) to investigate dynamic behavior of BHA. Using four straight beam strain gages, forces acting on the BHA were measured and transmitted using acoustic waves through the

drillstring. Deviation angle and WOB were varied during the experiments in the horizontal setup. Esmaeili et al. (2012) performed a study similar to the currently pursued in this study. Using sandstone rock sample with a roller cone bit and he found that 100 - 120 rpm is the optimum operating range at the maximum WOB of 800 N to provide better ROP with reduced vibrations (Fig. 2.11**)**. Patil and Teodoriu (2013b) designed a downscaled laboratory setup using law of similitude to study the effect of rotational speed, WOB, string length, string stiffness and inertia on the torsional vibration.

Figure 2.11: a) Laboratory scale rig b) Vibration sensor (Esmaeili et al. 2012)

Most of the field measurement deals with resonant frequencies and comparison of vibration amplitudes and frequencies. Field study by Wolf et al. (1985) suggested that resonant frequency of the system can be significantly lower than that of the natural frequency of the drillpipe and hence smooth drilling can be achieved if drilled at rotary

speeds above resonant speed. Dykstra et al. (1994) performed laboratory and field study on PDC and roller cone bits. They observed axial vibration in roller cone bits 3 times the rotary speed for field measurement. Full gauge stabilizers helped in reduction of harmful vibrations and raise the natural frequency of the encompassed drillstring. Jogi et al. (2002) calculated natural frequencies for all three modes of vibrations from different models and found a good match between measured and calculated values. A frequency-domain model of BHA lateral vibrations was developed by Bailey et al. (2008) and field data was matched with the model vibration indices in which correlation coefficients were found to be highly significant.

CHAPTER 3. EXPERIMENTAL INVESTIGATION

3.1 Experimental setup

A lab-scale drilling rig (Fig. 3.1) is constructed for competing in Drillbotics International Student Competition. OU Drillbotics team participated and won the competition in 2015. The following sections describe the rig setup and sensors installed, dividing them based on the systems: (i) Rig Structure, (ii) Hoisting System, (iii) Rotary System, (iv) Circulation System, and (v) Measurement, Instrumentation and Control System.

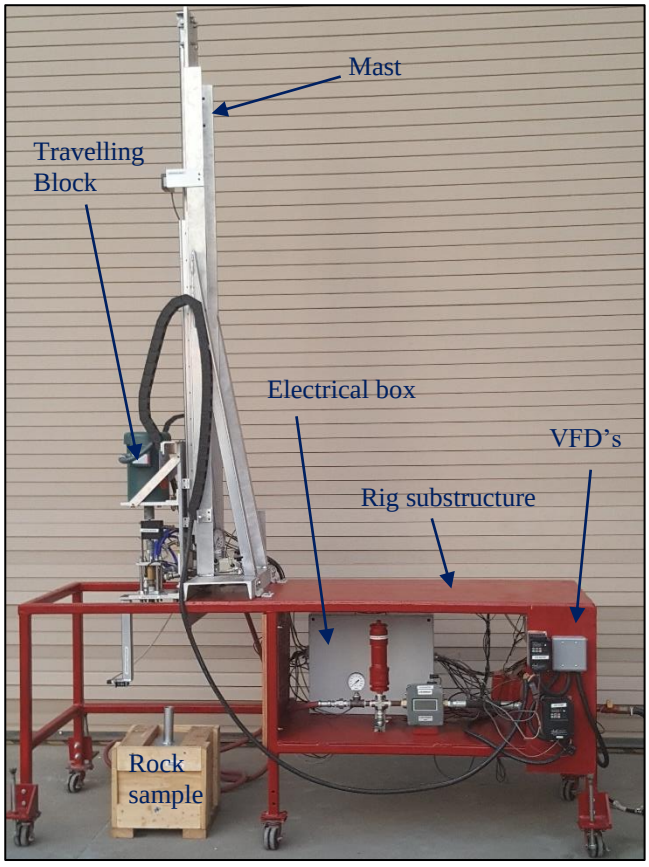

Figure 3.1: Lab-scale rig and its components

3.1.1 Rig Structure

Rig structure consists of three major components (Fig. 3.2): substructure, mast and travelling block.

Rig Substructure: In-house built substructure is used to have flexibility in the selection of dimensions, load ratings and design styles. The substructure is designed to pass through doors, so the rig could be used for future educational purposes. The rig substructure is constructed using 1½" square-iron tubing with overall dimensions of 84" x 27" x 36". To allow rig mobility, five commercial grade caster wheels are installed, each with load capacity of 1000 pounds. A 47" x 27" shelf made of ¼" thick iron sheet is added for installation of circulation system and electrical box. This left the rig with a space of 37" x 27" x 36" to accommodate the rock sample.

Mast: A mast of cantilever design is constructed out of Aluminum, as shown in Fig. 3.1. Constructing the mast with aluminum reduced the weight by 2.5 times to that made by steel. A 10-inch-wide C-Channel is supported by two 90 degree angle bars. The base is attached to the table with hinges for reclining and easy transport of the rig. Total rig height during operation is 7' 7" and 4' when mast is reclined.

Travelling Block: The travelling block slides on a pair of linear guide rails attached to the mast. Linear roller bearings or pillow blocks attached to the back of the travelling block provide near smooth motion. Two horizontal plates are bolted on the vertical plate. The upper plate acted as a mount for the AC motor and lower plate supported the swivel. A torque sensor is placed in between motor shaft and swivel. The total weight of the travelling block is measured to be 77.72 pounds.

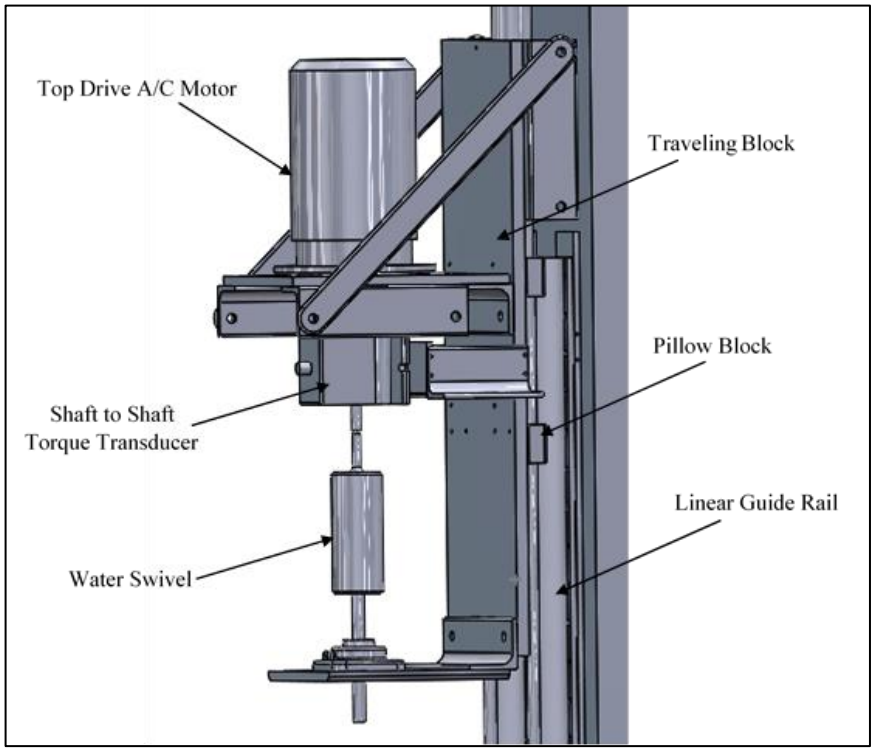

Figure 3.2: Diagram of travelling block assembly

3.1.2 Hoisting System

Hoisting system components include a double acting air cylinder, pneumatic lines, a couple of electropneumatic transducers and a compressed air supply line (Fig. 3.3). Regulated compressed air-line up to 130 psig is hooked up to the electropneumatic transducers. Two pneumatic lines from the transducers of maximum capacity 120 psig control the air pressure at the inlet ports of the double acting cylinder. The cylinder has a 1.125 inch bore and a 36-inch stroke length. The system has a capacity to hoist a load of 119.28 pounds.

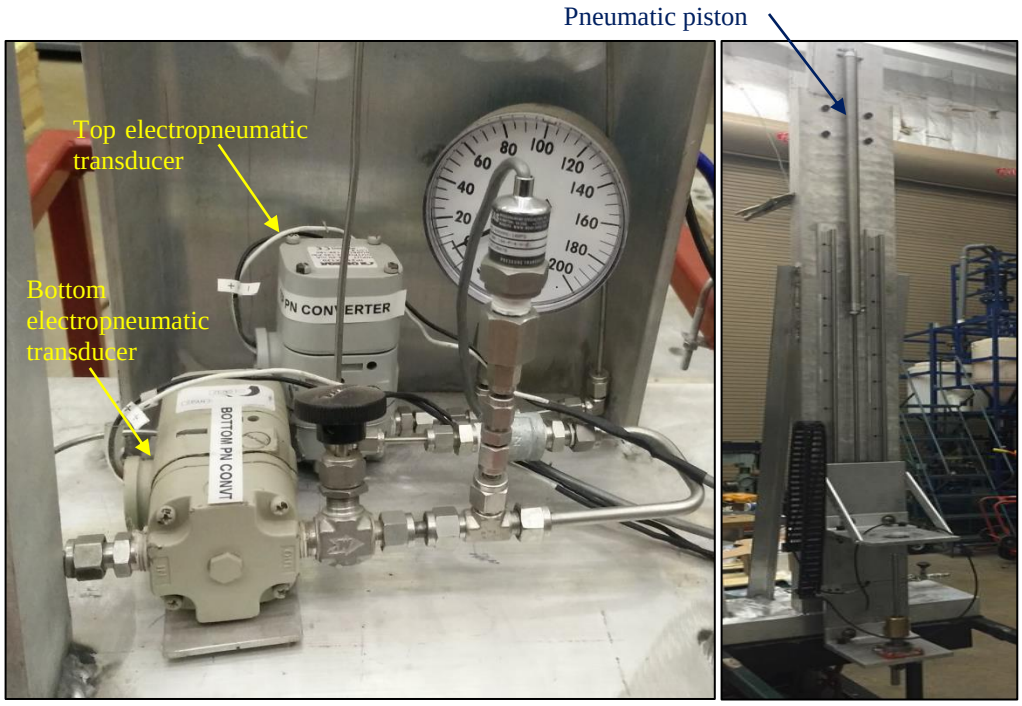

Figure 3.3: Electropneumatic transducers (left) and pneumatic piston (right)

3.1.3 Rotary System

A top drive system (1 HP motor with maximum speed of 1170 rpm) is installed on the motor-mount of the travelling block (Fig. 3.4). The motor shaft is connected to a torque sensor via a spring coupling. The torque sensor has a rotating shaft to shaft configuration with an operating speed of 5000 rpm. It is directly connected to the swivel via another spring coupling. The swivel is designed and fabricated in-house with pressure rating of 300 psi and brass outer body for corrosion resistance. The chrome plated rod is wear-resistant to the abrasion of the seals. Swivel rod is attached to an adapter at the base of the bottom plate. A four-bolt flange mounted thrust bearing prevents any load from being transmitted to the rotary assembly.

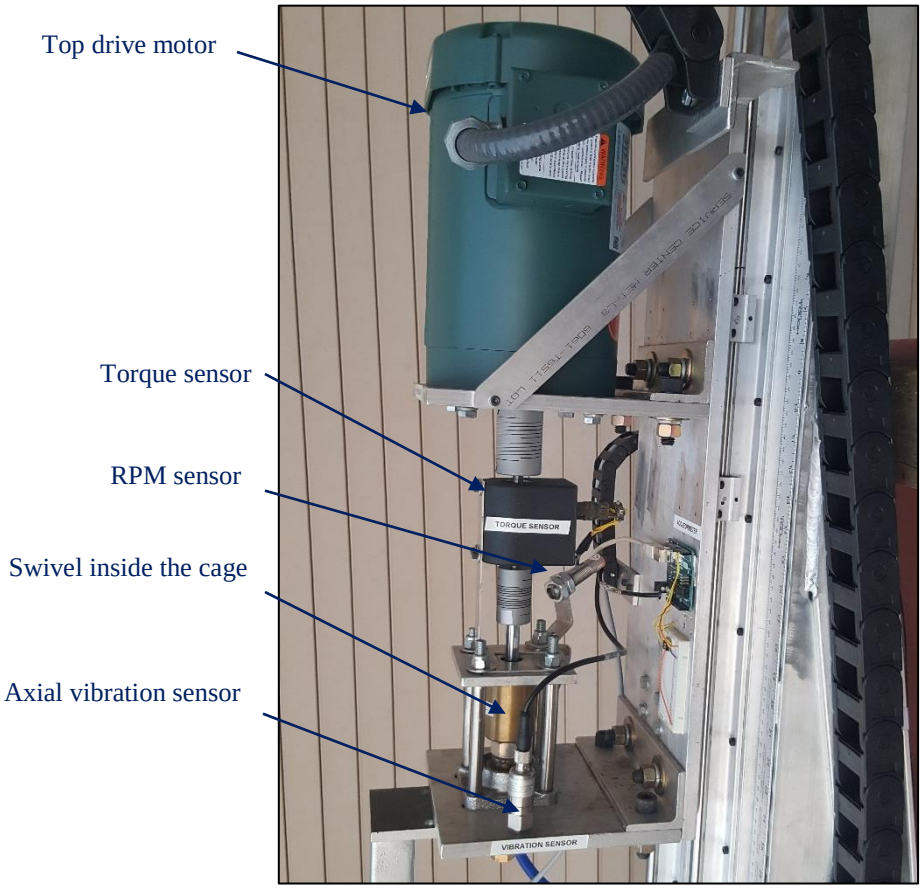

Figure 3.4: Travelling Block and its components

The drillstring assembly comprised of 3 parts, aluminum pipe, bit sub and bit (Figs. 3.5 and 3.6). The pipe is made of Aluminum 6061 with an OD of 0.375 inch and a thickness of 0.035 inch. Both ends of the pipe have 3/8" NPT male compression fittings attached on it. It is connected on one end to 3/8" NPT female brass adapter which is connected to the swivel rod and other end is connected to 3/8" NPT female bit sub. The bit sub is made from carbon steel and had 3/8" female NPT threads on both ends. A roller sleeve with OD of 1.088 inch and ID of 0.810 inch is slid upon the bit sub to act as a stabilizer and provide smooth rotation. It had a counter bore to place constriction of various sizes to change pressure drop in the system.

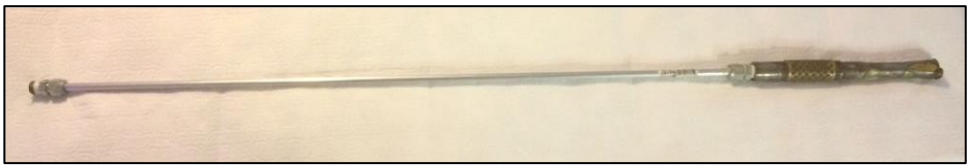

Figure 3.5: Picture of an assembled drillstring

Figure 3.6: Bit and Bit sub assembly

The bit was fabricated in house using carbon steel round bar and machined to replicate the Baker Hughes bit provided for the competition. The cutters were bought from vendors and the OD of the cutters available was 0.5 inch. The cutters are screwed on the cutter faces and are replaceable. Aluminum string is the weakest point in the complete assembly, hence following calculations were carried out to find out the operating constraints:

Barlow's Formula for Burst Pressure

$$P = \frac{2*Y*t*SF}{OD} \tag{3.1}$$

where Y is the minimum yield strength in psi, t is the thickness of the pipe in inches, OD is the outer diameter of pipe in inches and SF is safety factor.

$$P = \frac{2*40000*0.035*0.85}{0.375} = 6346.67\ psi \quad (3.2)$$

Euler's Buckling Theory

$$F_b = \frac{\pi^2 * E_x * I}{K * L^2} \quad (3.3)$$

where F_b is buckling force in lbf, E_x is modulus of elasticity in psi, I is area moment of inertia in inch^4, K is column effective length factor and L is the length of pipe in inches.

$$F_b = \frac{\pi^2 * 10000000 * 0.000546}{1 * 36^2} = 41.58 \text{ lbf} \quad (3.4)$$

Maximum Torsional Stress

$$T_{max} = \frac{\pi}{16} * \sigma_{max} * \frac{OD^4 - ID^4}{OD} \quad (3.5)$$

where T_{max} is maximum torque in in-lb, σ_{max} is maximum shear strength in psi, OD is outer diameter in inches and ID is inner diameter in inches.

$$T_{max} = \frac{\pi}{16} * 30000 * \frac{0.375^4 - 0.305^4}{0.375} = 174.77 \text{ in-lbf} \quad (3.6)$$

From the above calculations we can safely operate at a pressure of 6346.7 psi pressure while providing a force of 41.58 lbf on the string and 174.77 in-lbf torque. Maximum pump pressure is limited to 300 psi and torque limited to 62 in-lbf.

3.1.4 Circulation System

It is important to remove cuttings from the hole to drill further ahead. To accomplish this, water from the city line is directly connected to a roller pump with a pressure rating of 300 psi. The pump circulates the water down the drillstring assembly. A 1.5 HP 3-phase motor powers the pump. A flow meter is installed after the pump to measure flowrate. Pressure monitoring is done by a pressure transducer. Pressure fluctuation of up to 50 psi was observed due to intermittent flow supplied by the roller pump (Fig. 3.7). A pressure dampener is installed upstream to the flow meter. This provided smooth and stable flow. A gauge is mounted after the dampener to monitor pressure fluctuation. Rubber hose with a pressure rating of 300 psi connects the flow meter with the swivel. Drilling fluid from the swivel flows into the drillstring and comes out of the bit nozzles and out of the hole through the annulus. As the drilling fluid is just water, it was passed down the sewer line along with the cuttings and not recirculated.

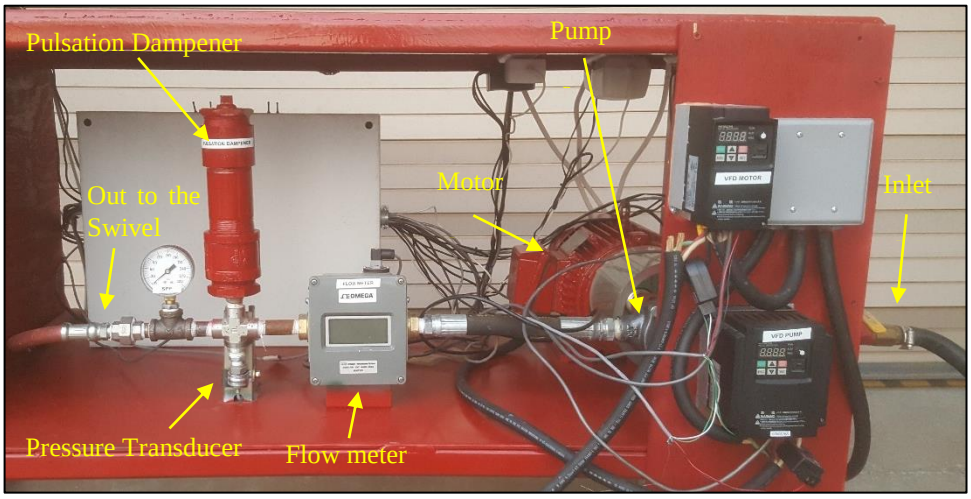

Figure 3.7: Circulation system

3.1.5 Measurement, Instrumentation and Control System

The Measurement, Instrumentation and Control system is the most important system in the automated rig. The sensors are mounted on the rig at various places for different functions. They provide analog data to the data acquisition module (Omega DAQ-3001). An electrical box was mounted at the bottom shelf for shielding the card and other signal conditioners from electrical interference. The data from the DAQ module transfers into the desktop computer, which is installed on the rig structure for control of the automated rig and storage and display of measurements. Excel-based VBA program is used for the operation of the rig. Schematic of the system is provided in the Fig. 3.8.

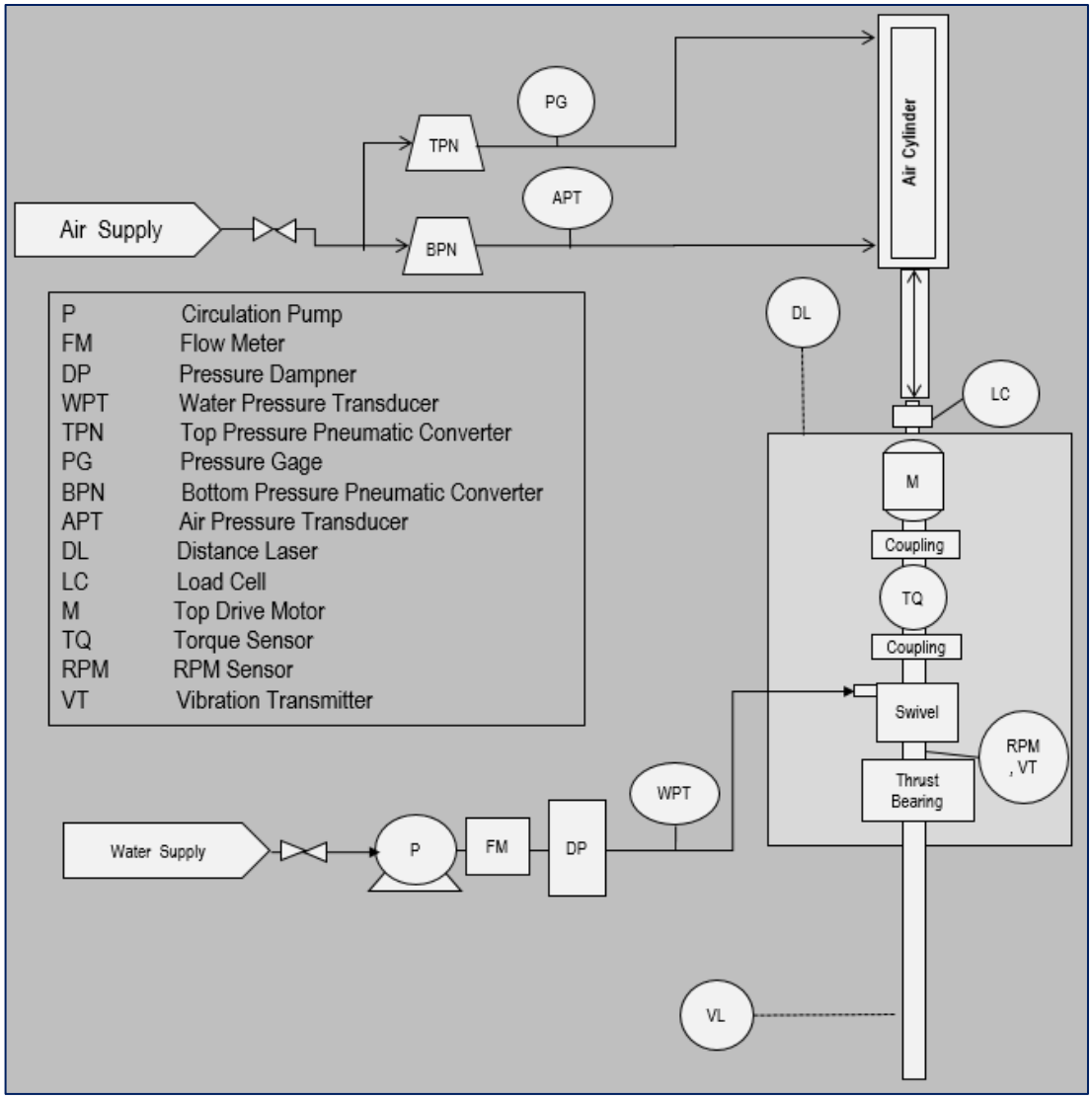

Figure 3.8: Schematic of the measurement, instrumentation system

Several sensors and control devices (displacement sensor, lateral vibration sensor, rpm sensor, torque sensor, axial vibration sensor, load cell, pressure transducers, flow-meter, variable frequency drives, electropneumatic transducers, signal conditioners, and data acquisition module) are installed on the rig to monitor performance of the drilling process.

i. Displacement Laser Sensor

An aluminum strip is attached to the top of the travelling block with a reflective tape stuck on it. A laser sensor (Banner LE55OUQ) is mounted about 0.5 inches above the travelling block on the mast. It can measure maximum displacement up to 39.37 inches with a resolution of less than 1 mm.

ii. Lateral Vibration Laser Sensor

To measure lateral vibrations of the drillstring, a photoelectric laser sensor (Wanglor OPT-2003) was used. The sensor can measure distance from 1.57 to 6.29 inches with an accuracy of less than 20 micrometers.

iii. Optical Rotational Speed Sensor

An LED-based, reflective type optical rotational speed sensor (Monarch ROS-P), which can measure up to 250,000 rpm, is mounted on the cage of swivel. Reflective tape is attached on the spring coupling between the swivel and torque sensor. The sensor is mounted at an angle so that the reflective area increases for better measurement. It provided a Transistor Transistor Logic (TTL) pulse output and has a range of detection up to 3 ft.

iv. Torque Sensor

It is assumed that torque measured by the torque sensor is the torque due to bit-rock interaction as the friction due to wall-bit sub interaction is considered negligible due to roller bearing cage. A rotating shaft to shaft torque sensor (Omega TQ513-62) has been mounted above the swivel with a torque rating of 62 inch-pounds. It provides a 2 mV/V output which is amplified using a signal conditioner. It has a maximum measuring capacity of 5000 rpm with a shaft diameter of 3/8 inch.

v. Axial Vibration Sensor

An axial vibration sensor (Dwyer VBT-1) is installed at the bottom plate of the travelling block adjacent to the flange mounted ball bearing. The sensor has a micro-electro-mechanical system which sends a voltage proportional to the vibration velocity to the data acquisition module. It measures vibration velocity from 0-25 mm/sec with an accuracy of ± 3%. The sensor is calibrated according to the vibration severity standards and provides a root mean square value of the vibration velocity.

vi. Load Cell

A load cell (Omega LC-203-100) is used to measure WOB during experiments. It has a range of measurement from 0-100 lbf with 2 mV/V output. The signal is amplified using a signal conditioner. It is installed between the piston rod and the travelling block at the back of the travelling block.

vii. Pressure Transducers

Pressure transducers are used to measure water and air inlet pressures. Air -line had a pressure transducer with a range of 0-100 psi and water line transducer had a range of 0-2500 psi. Both transducers send a 0-5 Vdc output.

viii. Flow-meter

A digital display flow meter (Omega FLR6315D) is used to measure water flow rate from 0-15 gpm. It has a maximum pressure rating of 3500 psig and an output range from 0-10 Vdc.

ix. Variable Frequency Drives

Variable frequency drives were used to control the three phase motors. A 1-HP rated Hitachi NES1-007LB is used to control the top drive Leeson 1 HP motor. A 2- HP rated Hitachi NES1-0015LB is used to control the motor for fluid circulation.

x. Electropneumatic Transducers

Electropneumatic transducers (Omega IP211X120-10V) were used to control the flow of air inside the piston. As the hoisting system is controlled with a dual acting cylinder two of them are installed. Along with control of air pressure, they also provided safety feature as the venting of air in case of power failure is very slow. They worked with a pressure output of 3-120 psi in a voltage supply range of 0-10 V.

xi. Signal Conditioners

Signal conditioners are used for various purposes. They have an output range of 0 - 10 Vdc. One is used to amplify the signal from Load cell and another from the torque sensor. Another signal conditioner (Monarch F2A3X) is used to convert the TTL signal from the optical sensor to analog form. It has rotational speed measuring range from 5 - 999990 with an output of 0 - 5 Vdc.

xii. Data Acquisition Module

A data acquisition module (Omega OMB-DAQ-3001) is used for data collection. It provides 16-bit resolution at 1 MHz frequency with analog input range of 0 to 10 Vdc. It had 16 single ended or 8 differential ended analog input channels and 24 digital input/output channels. 4 analog output channels are also provided along with 4 counter and 2 timers.

3.2 Test Material

Two rock samples (Fig. 3.9) were used for experimental investigation. The first one is classified as hard sandstone. UCS of the sandstone ranged from 5932 psi to 9544 psi with an average of 7500 psi (Table 3.1). The sample was bought from a stone supplying company and had an irregular shape and surface. Placing the guide shoe on the irregular surface would be hard and pilot hole could not be started as the rock sample was hard. So the rock sample was placed inside a wooden box and covered with cement and the surface flattened. A pilot hole was created in the cement and guide shoe installed.

Table 3.1: UCS test results for hard sandstone

Block I.D.	Load, lbf	Length, in	Width, in	Area, in^2	Psi
1	131250	4.04	4.13	16.69	7864
2	98000	4.06	4.07	16.52	5932
3	125000	4.02	4.09	16.44	7603
4	155000	4.03	4.03	16.24	9544
5	107500	4.07	4.07	16.44	6539
				Average	**7500**

The other sandstone sample can be classified as moderately hard sandstone with UCS ranging from 2000 to 5000 psi (Bavadiya et al. 2016). As the rock surface was smooth a pilot hole was easy to drill. As the sandstone was easy to drill, several holes were drilled in the 24 x 24 x 12 inches sandstone sample. For the purpose of this study, hard sample will be referred to as hard sandstone and moderately hard sample will be referred to as soft sandstone.

Figure 3.9: Rock sample on left is soft sandstone and on the right is the hard sandstone

Figure 3.10: Holes drilled in soft sandstone (L) and hard sandstone (R)

3.3 Experimental Matrix

Tests were conducted varying WOB and rotational speed (**Table 3.2**). The minimum WOB was 10 pounds because below 8 pounds measurements were not accurate due to static friction. As per Euler's buckling force calculations, a maximum of 41.58 lbf WOB should be applied. Any force more than this value will buckle the pipe but the end

of pipe is restrained by the borehole wall and hence actual force which can be applied before buckling increases. When WOB was higher than 50 pounds, the stress level at the compression fitting increased and resulted in the development of crack in the pipe at higher rotational speed.

Table 3.2: Experimental Matrix

	Rotational Speed (rpm)										
	50	**100**	**150**	**200**	**300**	**400**	**500**	**600**	**700**	**800**	**900**
WOB (lbf)	10	10	10	10	10	10	10	10	10	10	10
	20	20	20	20	20	20	20	20	20	20	20
	30	30	30	30	30	30	30	30	30	30	30
	40	40	40	40	40	40	40	40	40	40	40
	50	50	50	50	50	50	50	50	50	50	50

Powerpak handbook by Schlumberger (2004) lists the current mud motors in the market. At the maximum rotational speed of the motors, the flow rate is 640 rpm. Along with surface rotational speed of 200 rpm, a maximum rotational speed of 840 rpm can be achieved at the bit. The vibrations at 900 rpm were high enough to damage the spring couplings. Hence, set of experiments on hard sandstone were not carried out at 900 rpm.

3.4 Experimental Procedure

The rig and all its components were powered on and the Excel program initiated. The program had a separate sheet for reading input variables of the experimental run. The variables changed for the set of experiments are rotational speed and WOB. To start the experiment, first a pilot hole of 1.25-inch diameter and 1-inch depth was drilled into the rock sample using a coring bit and hammer-chisel to insert a guide shoe in the hole. The 6-inch long guide shoe acted as an initiated hole and prevented bit walking. Using a level indicator, the rock sample was adjusted to be horizontal. The drillstring was attached to

the swivel adapter and rig was then slid over the rock to align the drillstring and the guide shoe. Using the leveling screws the rig was jacked up to be horizontal.

The inlet air and water lines were connected and opened up. Water was circulated at pressure of 145 psig and flow rate of 3 gpm. Cutting effect due to water jet from nozzle is assumed negligible as pressure drop across the nozzles is 75.2 psi which is calculated using Eqn. (3.4). Once all experimental variables were set, the program was initiated using the VBA start button. The first step of the program was to hoist the travelling block to the topmost position. At this point a safety bar used to keep the travelling block hoisted was taken away. The travelling block slowly lowered down and once the bit was inside the guide shoe, top-drive motor and pump motor got activated and string started to rotate along with pressurized water inside the pipe. The bit gradually touched the rock and drilling process began.

A trial run was carried out to check if the systems were working properly and data was being collected. A couple of millimeters were drilled during the trial run so that the hole got initiated.

After a trial run, experimental runs were carried out. Each experiment was run for 6 min and stopped using the stop button in the program. The pump stopped pumping fluid and drillstring stopped rotation. Travelling block was gradually lifted up to the topmost position. After that new experimental variables were set and the next run was carried out. Experiments were performed on two different rock samples.

3.5 Sensor Calibration and Data Collection

Data was continuously collected by the data acquisition module and stored in an excel sheet. An average of 120 data points were collected in each test with an average of

1 data point every 3 seconds. The data of interest were WOB, rotational speed, torque, axial vibrations, lateral vibrations and ROP. Different plots were generated against variables of interest to observe dependency and behavior of the variable under investigation.

3.5.1 WOB and Rotational Speed Measurements

WOB was an independent variable with respect to this investigation. WOB was measured using a load cell attached to the back of travelling block connecting the piston. To calibrate WOB sensor, first the rig was slid over a weighing scale. A set number of values were entered for voltage sent to the bottom pneumatic convertors. A constant voltage of 2 volts was sent to the top electropneumatic transducer to provide a constant pressure of 20 psig resistance against erratic bouncing and to provide a constant friction between piston and cylinder walls in either direction. Reading on the weighing scale was recorded as WOB. Initially the WOB calibration was performed in a static condition. It was observed that WOB reading during the experiment was different than the expected values based on calibration. It was assumed that the change of conditions from static to dynamic was the cause of difference. Hence to simulate dynamic conditions while calibration, rig was constantly hammered down with a mallet to cause the rig to vibrate and negate static friction. The stabilized reading on the scale was used for calibration. But hammering still did not exactly replicate the vibrations happening during the drilling process and hence the WOB measurement by the load cell was different from expected based on the calibration. Hence average value of the WOB was calculated for complete experimental run and considered as the WOB which is being exerted on the rock for cutting process.

The average WOB observed had a change of 19.9 % to -20.6 % from the expected input values. In actual drilling process, the WOB fluctuates. As the drilling proceeds, the WOB decreases and drillers lower the drillstring to maintain the level of WOB. Hence, ± 20 % change from the set point is acceptable. Jet impact force was calculated below, which was subtracted from the measured WOB from the DAQ card.

Pressure Drop Across the Bit

$$\Delta P_b = \frac{8.311*10^{-5}\rho q^2}{C_d^2 A_t^2} \tag{3.7}$$

where ρ is density of fluid in ppg, q is flow rate in gpm, C_d is coefficient of discharge and A_t is total area of nozzels in in^2.

$$\Delta P_b = \frac{8.311*10^{-5}*8.33*3^2}{0.95^2*0.00958^2} = 75.32 \text{ psi} \tag{3.8}$$

Jet Impact Force

$$F_j = 0.01823 * C_d q\sqrt{\rho \Delta P_b} \tag{3.9}$$

where C_d is coefficient of discharge, q is flow rate in gpm, ρ is fluid density in ppg, ΔP_b is pressure drop across the bit.

$$F_j = 0.01823 * 0.95 * 3\sqrt{8.33 * 75.32} = 1.30 \text{ lbf} \tag{3.10}$$

Rotational speed data was obtained from the optical rotational speed sensor which was calibrated using a handheld rotational speed sensor. At lower rotational speed the

error was around 8 % and at higher rotational speed it reduced to 0.5 %. So, at lower levels the set point was decreased by 4 to compensate for the error.

3.5.2 Torque, Axial and Lateral Vibration Measurements

A rotating shaft to shaft torque sensor was placed in between the motor and swivel with a spring coupling on each end. Torque was calibrated using a torque wrench. When run at idle conditions without any drilling action, torque reading obtained was assumed to be friction. That extra torque of 1.114 inch-pounds was assumed to be a side force or the friction inside the swivel and other rotating parts such as the flange mounted ball bearing.

A laser displacement sensor was attached to the mast to detect the magnitude of lateral vibrations. It was aimed at the center of the drillstring such that the pipe was always in range of the laser. The laser sensor was kept 4 inches away from the center of pipe. NPT connections are inherently non-concentric and causes non-alignment of pipe. The pipe wobbled due to non-alignment and it oscillated far and near to the sensor. Hence, there was a negative and a positive value for displacement. The most negative value of the displacement was used as a reference zero and complete data was shifted towards positive with -0.24165 inch as a reference zero. Greater the magnitude, pipe travelled farther away from the sensor indicating higher lateral vibrations.

An axial vibration sensor was attached to the bottom plate of the travelling block. It had micro-electro-mechanical system inside to detect the vibration speed and send a proportional voltage signal for measurement. The sensor came calibrated from the manufacturer and it has a direct vibration-velocity to voltage relationship provided by the manufacturer. Some of the measurements for vibration velocity exceeded 25 mm/s. The

sensor has a capacity to measure 0-25 mm/s velocity within ± 3 % accuracy. Measurements above 25 mm/sec may have less accuracy.

3.6 Results

ROP was calculated from the drilled depth. As the hard sandstone was difficult to drill the sensor could not measure any significant change in drilled depth in 6 minutes. Hence, ROP data for hard sandstone is not presented (Table 3.3). Soft sandstone ROP data (Table 3.4) was collected and analyzed for effect of vibrations and other parameters. Table 3.3 shows the averaged data obtained after from experiments on hard sandstone.

Table 3.3: Results for hard sandstone

Rotational speed (rpm)	WOB, lbf	Torque, in-lbf	Axial_Vib, mm/s	Deflection, in
50	6.54	0.42	2.75	0.0163
	12.41	0.57	2.34	0.0249
	19.55	1.25	2.98	0.0379
	30.53	2.18	3.43	0.0658
	36.76	1.68	4.54	0.0286
100	6.47	0.51	3.73	0.0242
	11.90	0.73	3.60	0.0344
	19.70	1.25	4.66	0.0536
	27.53	1.96	5.27	0.0518
	34.82	1.15	6.45	0.0250
150	6.34	0.73	5.28	0.0188
	16.00	0.43	6.13	0.0280
	18.62	1.27	5.87	0.0424
	27.36	2.17	7.09	0.0242
	36.06	1.22	8.73	0.0170
200	6.04	0.70	6.83	0.0282
	11.44	1.26	8.01	0.0168
	17.78	2.41	14.31	0.0376
	25.26	3.73	21.26	0.0267
	37.47	1.49	11.02	0.0190
300	6.27	1.03	8.36	0.0345
	11.07	2.04	22.43	0.0246
	18.28	2.74	25.75	0.0247
	27.89	4.63	27.41	0.0669

Rotational speed (rpm)	WOB, lbf	Torque, in-lbf	Axial_Vib, mm/s	Deflection, in
	38.88	2.03	15.82	0.0100
400	6.99	1.38	13.19	0.0397
	13.00	2.04	16.47	0.0405
	19.00	1.85	15.21	0.1012
	28.39	1.80	17.14	0.0829
	38.62	2.45	18.04	0.0464
500	6.20	1.45	13.85	0.0563
	12.48	1.75	13.40	0.0739
	18.45	2.21	16.68	0.0983
	29.15	2.37	20.25	0.1313
	37.91	3.24	21.88	0.1187
600	6.85	2.04	24.04	0.0722
	12.72	2.06	14.37	0.0853
	19.92	2.44	19.94	0.1071
	28.46	2.64	23.20	0.1139
	37.22	4.22	25.73	0.2268
700	6.48	1.47	16.88	0.1066
	12.69	2.39	18.80	0.0822
	18.80	2.49	21.46	0.1087
	28.59	2.78	25.34	0.1273
	38.12	3.69	25.14	0.3321
800	5.79	1.49	16.25	0.0664
	11.52	2.32	17.70	0.1287
	19.03	2.74	23.75	0.1458
	26.68	2.87	25.77	0.1215
	39.31	3.69	26.45	0.3225

Table 3.4: Results for Soft Sandstone

RPM	WOB, lbf	Torque, in-lbf	Axial_Vib, mm/s	Deflection, in	ROP, in/hr
50	8.85	0.61	1.43	0.0281	0.61
	16.87	1.27	2.41	0.0361	0.60
	21.13	2.77	2.89	0.0402	0.66
	29.16	3.47	1.48	0.0350	0.29
	37.98	4.37	1.61	0.0206	0.38
100	9.73	0.72	2.61	0.0347	0.76
	16.66	1.64	4.22	0.0411	0.88
	20.98	2.93	5.28	0.0445	1.49
	27.56	3.45	2.95	0.0307	0.45
	34.74	4.66	3.23	0.0236	0.94
150	10.04	0.92	3.84	0.0346	1.30
	16.67	1.88	5.31	0.0342	0.96
	20.42	3.10	6.69	0.0466	1.70
	28.52	3.98	4.76	0.0306	1.15
	40.22	4.82	4.96	0.0650	0.89
200	10.04	1.17	4.90	0.0312	1.53
	16.93	2.12	7.04	0.0416	1.24
	21.08	2.88	6.75	0.0552	1.09
	28.45	4.24	6.77	0.0344	1.41
	38.75	5.70	6.51	0.0300	1.57
300	8.35	1.35	6.04	0.0350	2.35
	16.99	2.50	8.86	0.0418	1.96
	22.13	3.85	10.35	0.0446	3.06
	30.65	5.01	10.05	0.0456	2.81
	40.59	6.02	9.89	0.0341	3.07
400	8.62	1.61	8.39	0.0338	2.91
	17.22	2.85	15.05	0.0448	3.08
	22.02	4.15	13.84	0.0474	4.23
	32.00	5.17	13.66	0.0498	4.38
	41.44	6.35	12.15	0.0277	3.66
500	9.37	1.85	8.85	0.0351	3.83
	13.42	2.93	12.45	0.0421	3.77
	24.18	4.65	14.28	0.0435	5.22
	31.13	5.23	16.27	0.0599	5.29
	42.12	6.62	15.04	0.0274	4.97
600	9.72	2.32	26.50	0.0352	6.83
	13.71	3.49	24.01	0.0392	7.01
	24.70	4.76	14.92	0.0427	6.24
	30.06	5.25	16.94	0.0596	6.53

RPM	WOB, lbf	Torque, in-lbf	Axial_Vib, mm/s	Deflection, in	ROP, in/hr
	42.26	6.83	16.43	0.0389	6.61
700	10.96	2.14	19.98	0.0440	7.16
	14.34	3.46	23.03	0.0352	8.39
	24.65	5.13	23.70	0.0605	10.38
	35.11	6.54	24.82	0.0515	13.02
	47.38	8.01	21.80	0.0277	10.64
800	10.58	2.04	10.35	0.0364	5.70
	15.40	4.15	21.20	0.0904	3.80
	24.00	4.83	18.36	0.0455	8.55
	34.35	6.39	20.52	0.0428	11.74
	46.33	7.88	21.15	0.0192	12.09
900	7.03	2.26	10.22	0.0347	1.90
	14.80	3.33	13.66	0.0430	4.25
	21.74	4.50	15.27	0.0494	5.07
	33.16	6.27	16.55	0.0609	7.69
	48.69	8.26	22.22	0.0477	13.62

4. DATA ANALYSIS AND DISCUSSIONS

Data was collected from the point where the bit touches the rock to the point when the program was stopped. An average of those data was calculated and stored. Average values of torque, axial vibrations and lateral vibrations were plotted against rotational speed and WOB separately. A trend of data was analyzed based on the plots. With increase of rotational speed, change of torque, axial and lateral vibration was observed.

4.1 Torque Measurements

Stick slip oscillations are torsional vibrations, which occurs in a long drillstring or a short flexible one to absorb the rotational energy and impart it at a later stage. As the drill pipe used in the experiments is a rigid short pipe, no stick slip was observed. The response of torque with varying WOB and rotational speed is discussed here.

Hard Sandstone: Torque predominantly increased (Fig. 4.1) with rotational speed at constant WOB. In the range of 200 to 300 rpm, there was a sudden increase in torque for some cases (18.91 and 27.98 lbf) which then decreased. This behavior is unexpected. It could be attributed to material heterogeneity resulting in abnormally hard thin layers which unexpectedly increased the torque. Nonetheless, the general trend is a gradual increase in torque with rotational speed at low speeds (less than 500 rpm) and slight increase at high speeds (more than 500 rpm). No oscillation of torque was observed indicating absence of stick-slip. Increase in WOB at constant rotational speed gradually increased the torque (Fig. 4.2) except for low rotational speed measurements (Figs. 4.3) which is unexpected.

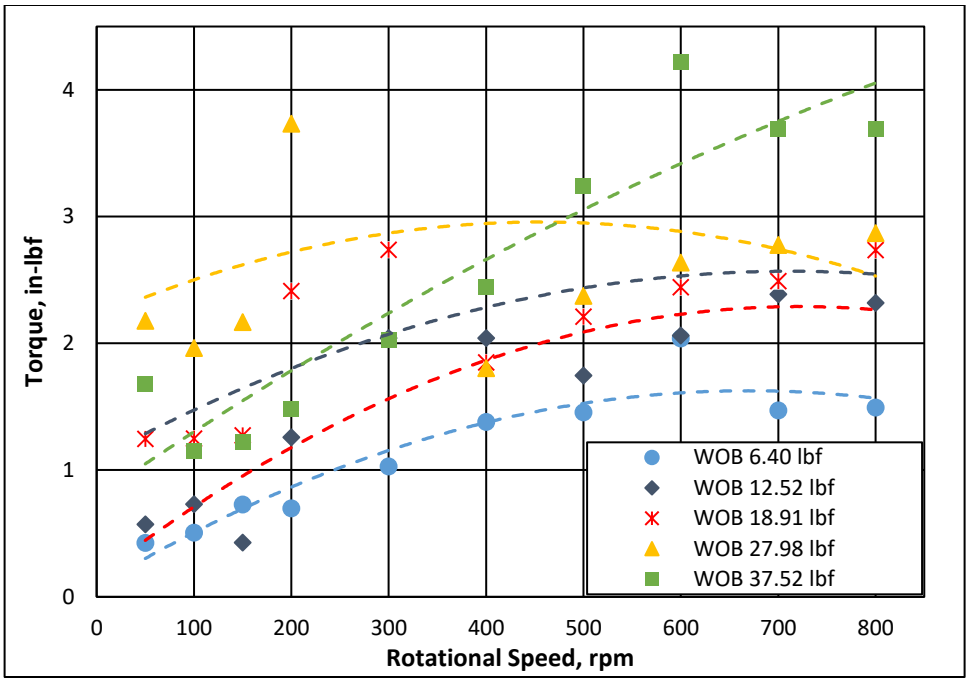

Figure 4.1: Torque vs. rotational speed at constant WOB (hard sandstone)

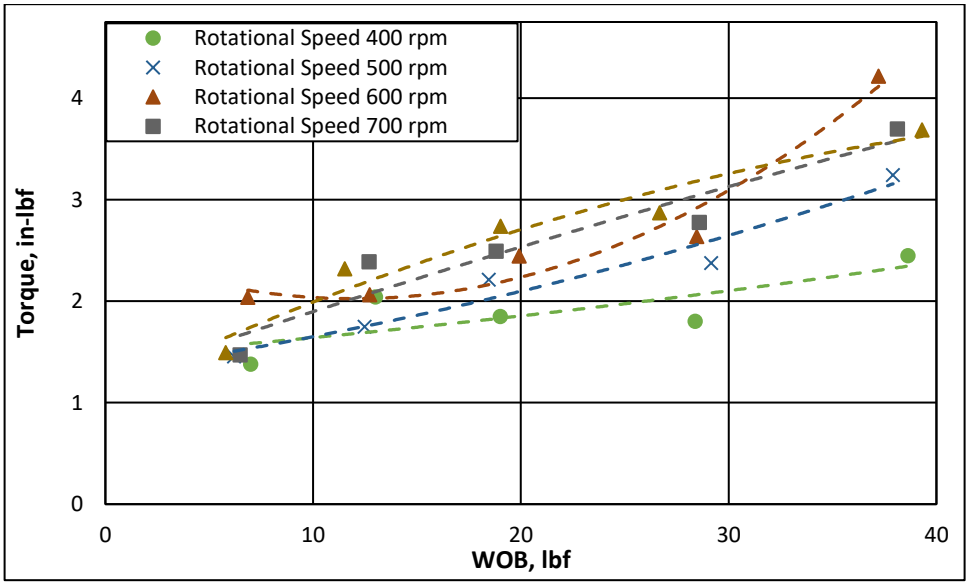

Figure 4.2: Torque vs. WOB at constant rotational speed (hard sandstone)

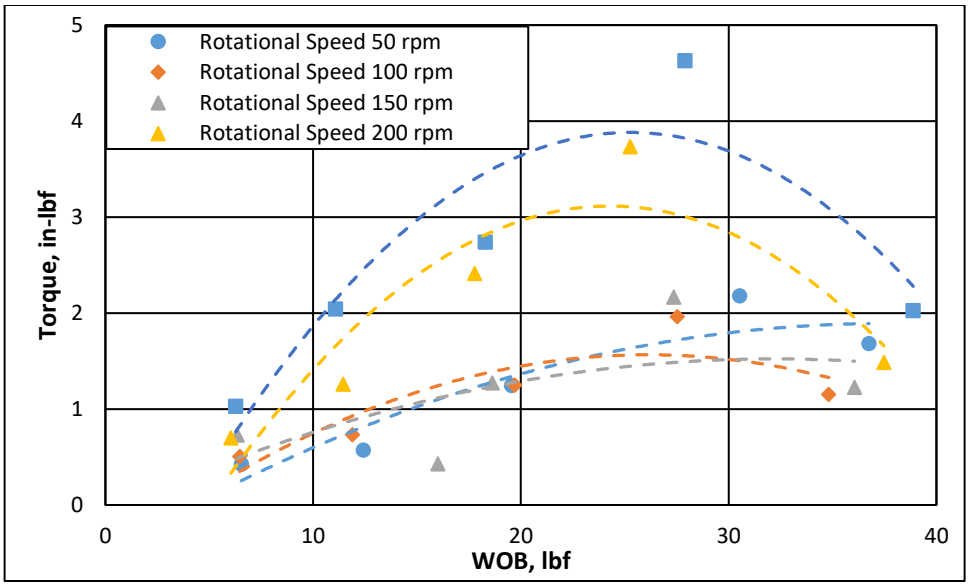

Figure 4.3: Torque vs. WOB at constant rotational speed (hard sandstone)

Soft sandstone: Consistent with hard stone measurements, mostly a gradual increase (Fig. 4.4) in torque was observed with rotational speed at constant WOB. The increase diminished at high speeds (more than 500 rpm) and even in some cases trend reversal was observed. The reason for such a trend could be the decrease of sliding friction coefficient at high speeds. Burwell and Rabinowicz (1953) performed experiments to find the nature of coefficient of friction between metal to metal contact. They observed that at very high speeds the sliding friction coefficient decreases. With decrease in friction coefficient the torque required to counter friction force would decrease. Like hardstone, no oscillation of torque was observed that indicate stick-slip. There is a clear and distinct torque trend with WOB at constant rotational speed (Figs. 4.5 and 4.6).

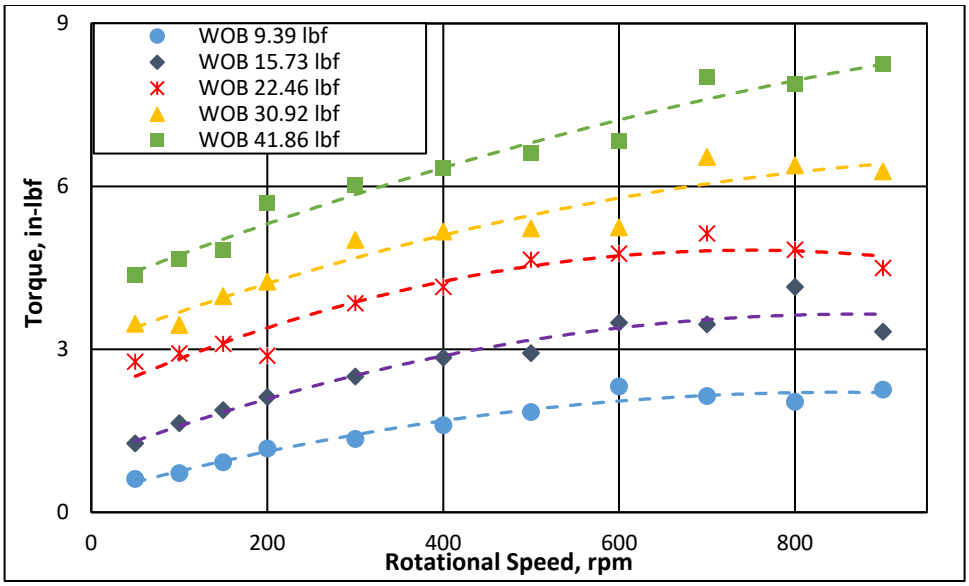

Figure 4.4: Torque vs. rotational speed at constant WOB (soft sandstone)

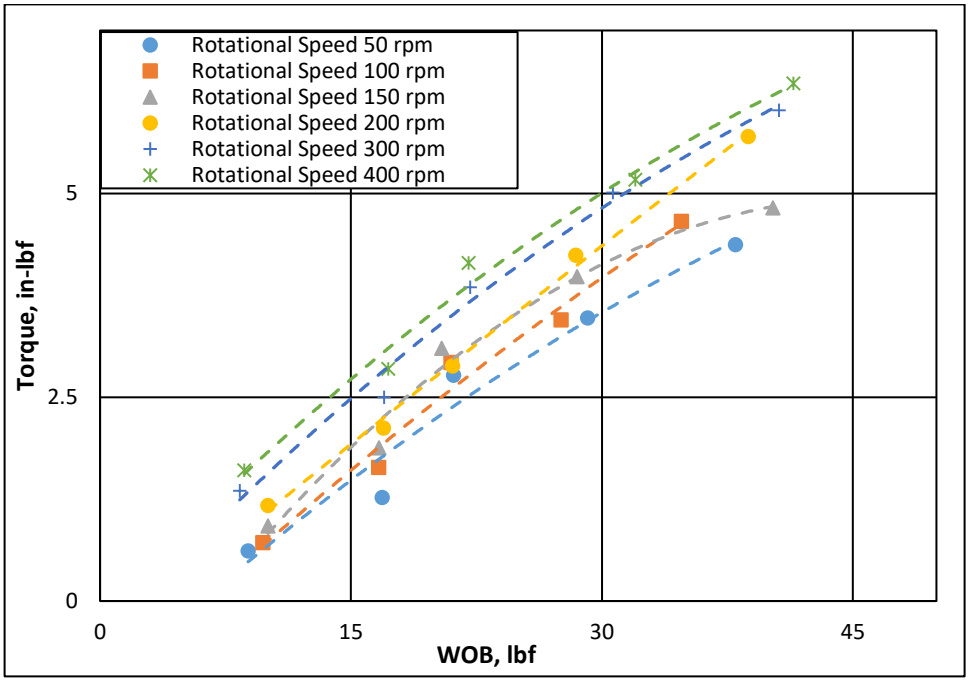

Figure 4.5: Torque vs. WOB at constant rotational speed (soft sandstone)

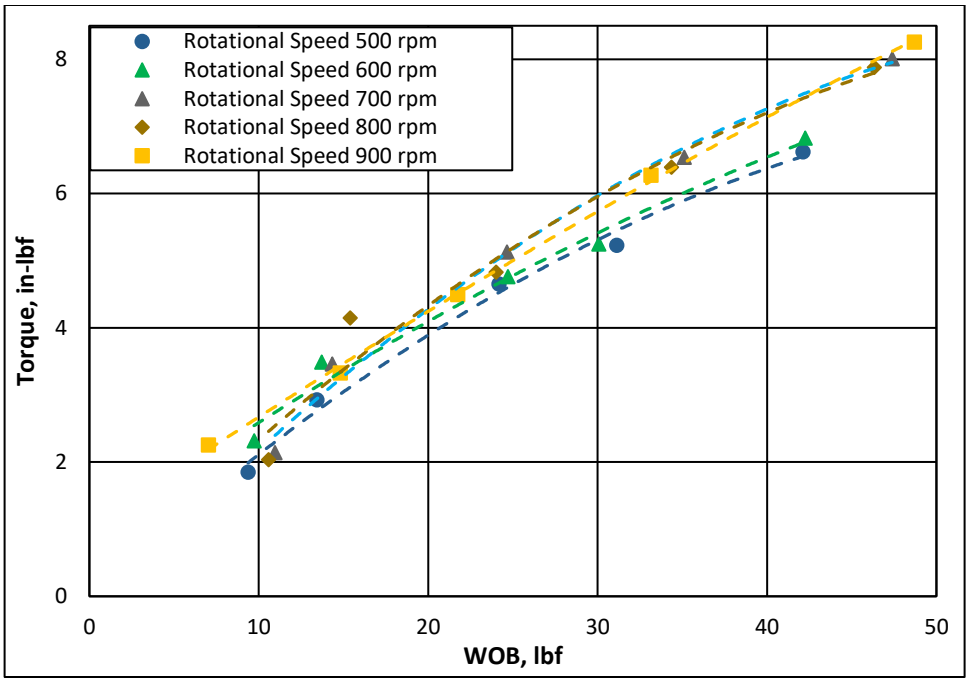

Figure 4.6: Torque vs. WOB at constant rotational speed (soft sandstone)

4.2 Comparison of Model with Measurements

ROP data was available only for the soft sandstone and hence torque prediction is made for soft sandstone experiments based on the model developed by Detournay and Defourny (1992). Input parameters for the model are presented in Table 4.1.

Table 4.1: Parameters used for calculating analytical torque

Parameter	Symbol	Value	Source
Radius of bit, in	a	0.5625	Measured
Coefficient of friction	μ	0.82	Berea Sandstone
Intrinsic specific energy, psi	ϵ	4641	Berea Sandstone
Drilling strength to rock strength ratio	k	0.8	Berea Sandstone
Bit constant	γ=l/2a	1.39	Estimated
Length of cutting edge	l	1.57	Estimated

Comparison performed between model predictions and experimental measurements show discrepancies (Figs. 4.7 and 4.8) ranging from 0.6 to 374.85%. At low WOB the error ranges from 0.6% to 374 % compared to an average of 105 % at high WOB. It can be observed from plots (Figs. 4.7 and 4.8) that at low WOB, torque decreased with rotational speed. This can be attributed to the change in bit constant due to no cutter space at the center of the bit. Due to the no cutter space, there is a protrusion at the center of the hole which creates unwanted lateral and axial vibrations. The dimensionless length or the contact surface decreased at higher rotational speed due to vibrations, decreasing the depth of cut at higher rotational speed and hence decreasing the predicted torque. At higher WOB, it is assumed that the tip of protrusion gets crushed and hence maintained a constant dimensionless length. Below given is the table of parameters used to obtain analytical torque values.

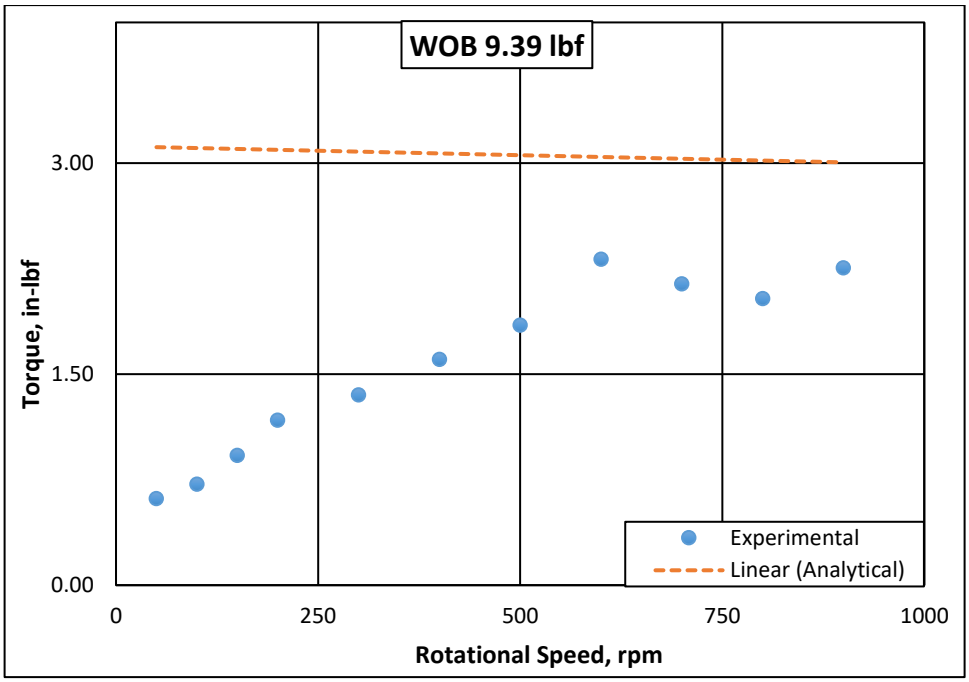

Figure 4.7: Torque vs. rotational speed at an average WOB of 9.39 lbf

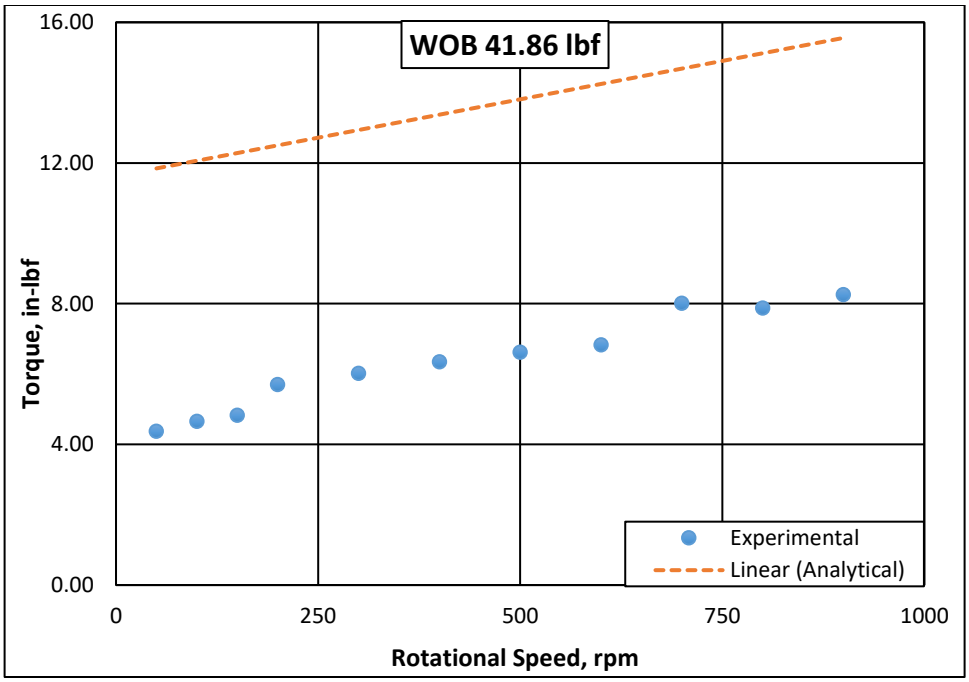

Figure 4.8: Torque vs. rotational speed at an average WOB of 41.86 lbf

Parametric sensitivity was carried out to determine the influential parameters and their impacts. Input parameters were changed and their effects on torque were investigated. Drilling strength to rock strength ratio was varied from 0.5 to 2.1. As can be observed from Figs. 4.9 and 4.10, the change in torque due to this parameter is insignificant. In an idealized cutting process, the bit traces the cutting locus as seen in Fig. 2.4. When frictional process is involved, the torque response is primarily governed by $\mu\gamma$ which is discussed further in the section.

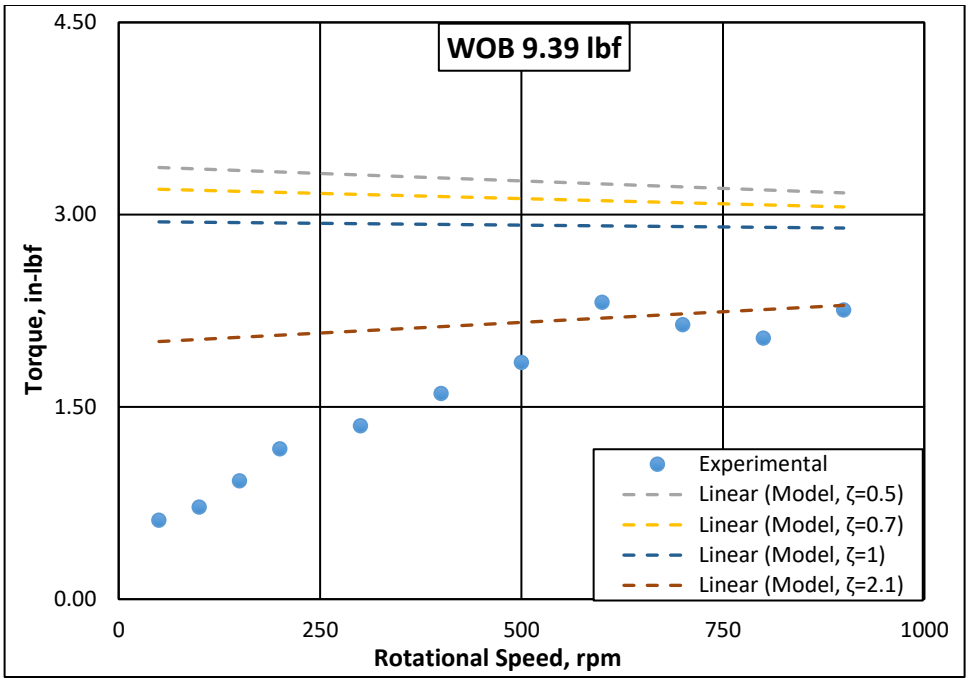

Figure 4.9: Torque vs. rotational speed at an average WOB of 9.39 lbf, ζ varied from 0.5 to 2.1

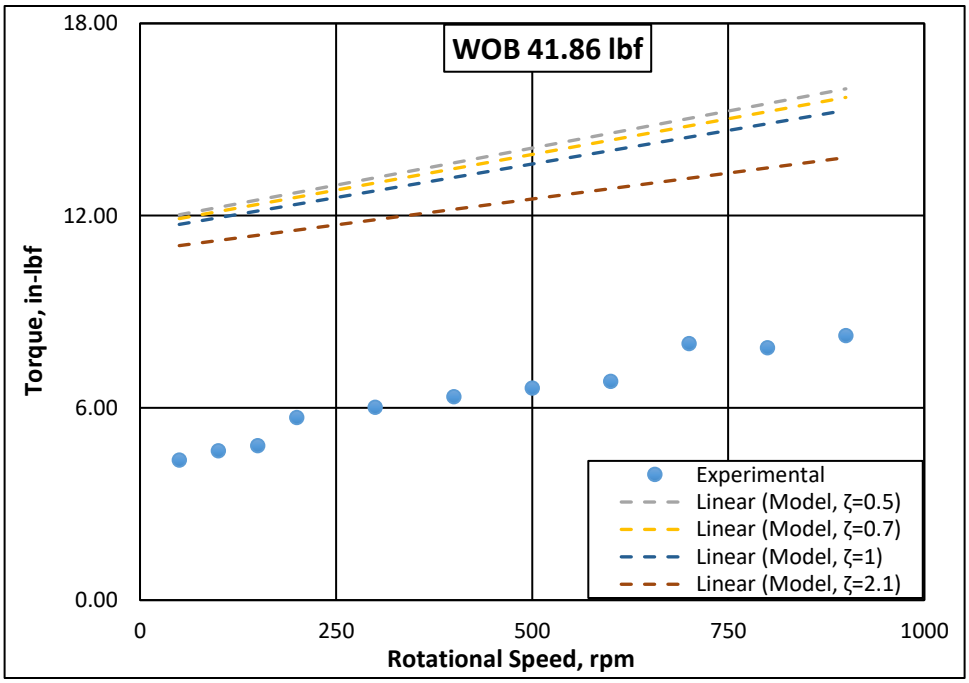

Figure 4.10: Torque vs. rotational speed at an average WOB of 41.86 lbf, ζ varied from 0.5 to 2.1

Intrinsic specific energy of the sandstone sample is assumed to be similar to Berea sandstone based on the available UCS data. Specific energy is varied from 150 psi to 10000 psi and results are presented in Fig. 4.11. Intrinsic specific energy is not a significant parameter for estimating torque. No significant change in torque is observed from change in specific energy.

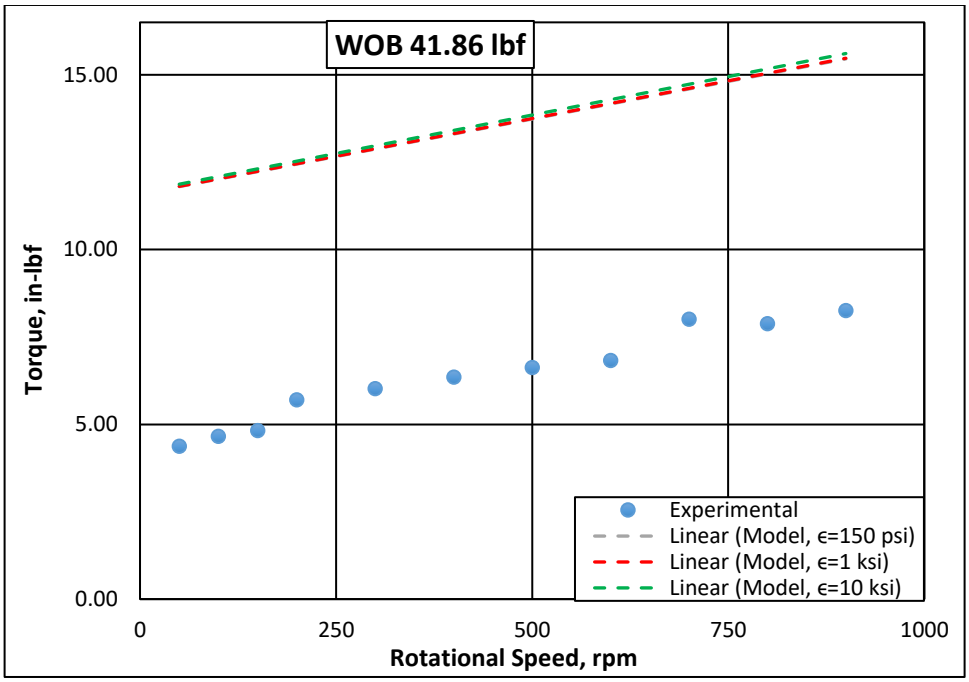

Figure 4.11: Torque vs. rotational speed at an average WOB of 41.86 lbf, ϵ varied from 150 psi to 10000 psi

Bit constant was varied from 0.25 to 1.39 and the results are presented in Fig. 4.12. It can be seen from the plot that bit constant of 0.6 accurately matches the prediction with the experimental data. Moreover, coefficient of friction was varied from 0.37 to 0.85 (Fig. 4.13) and friction coefficient of 0.37 matched the prediction with the actual torque. Almost 55 % reduction of coefficient of friction from the base case provides accurate prediction.

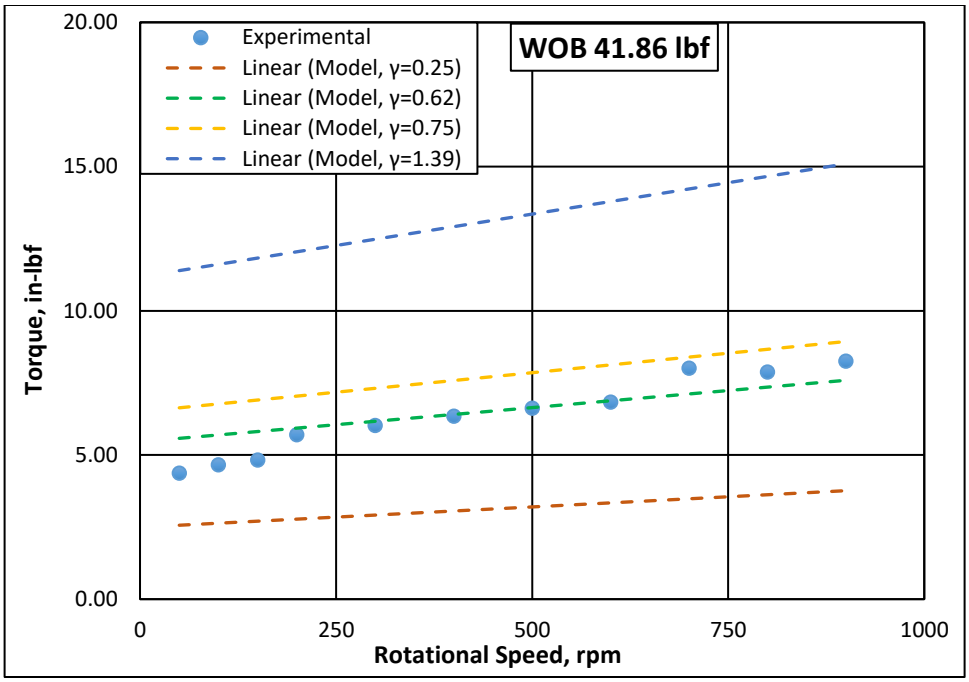

Figure 4.12: Torque vs. rotational speed at an average WOB of 41.86 lbf, γ varied from 0.25 to 1.39

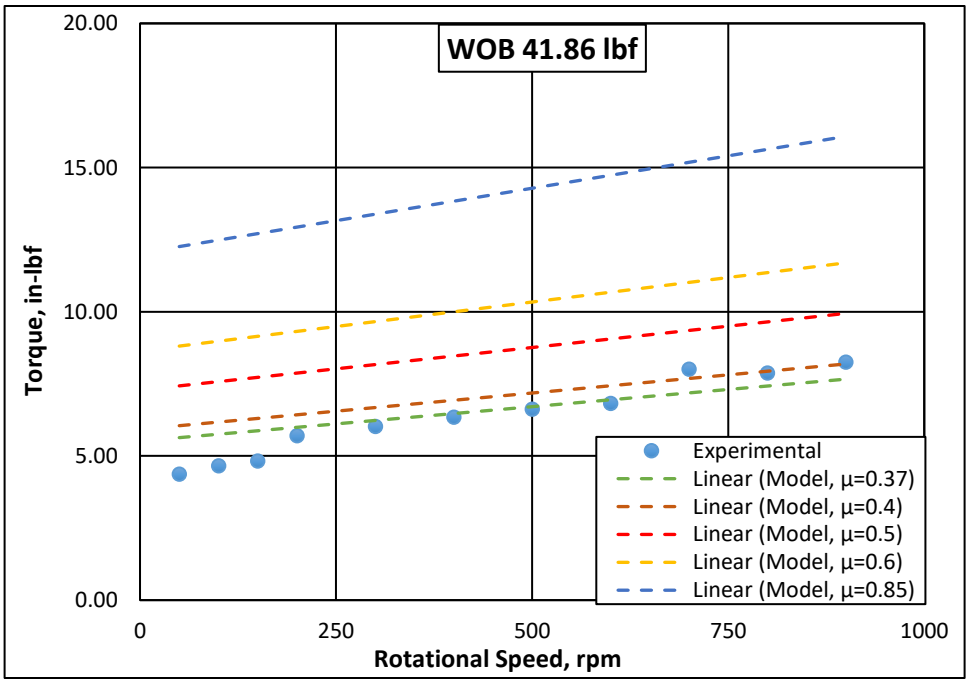

Figure 4.13: Torque vs. rotational speed at an average WOB of 41.86 lbf, μ is varied from 0.37 to 0.85

Looking closely at Eqn. (2.7), decrease in 55% of either friction coefficient or bit constant can produce similar results. Coefficient of friction for base case was assumed to be 0.82, which was for dry interaction between Berea sandstone and diamond cutter. In the study, interaction between the rock and carbide cutter is lubricated with water, decreasing the friction coefficient. For a bladed bit, the bit constant is generally greater than 1. Hence, if we assume that the bit constant for the base case is correct then it is reasonable to assume 0.37 as the friction coefficient between the sandstone sample and the cutter.

Drilling Specific energy (E) and drilling strength (S) are calculated using the model presented in Section 2.2. The data is presented as E-S plot and linear regression is applied (Fig. 4.14). Comparing the linear regression line with Eqn. (2.10), we get $\mu\gamma$ = 0.4759. If γ is assumed 1, then μ = 0.4759 and if γ is assumed 1.39, then μ = 0.34. As per the parametric study, it can be observed that μ = 0.37 matches the experimental results; and hence, it would be reasonable to assume that the bit constant is 1.29 than the assumed value of 1.39.

The ordinate of the lower left data point represents the upper bound on the intrinsic specific energy which is equal to 3040 psi which forces the condition that β must be negative. Since neither of the variables of β can be negative, the second most lower left data point is selected which gives a value of 12282 psi which is higher than the estimated range of 2000 to 5000 psi. Friction angle is calculated as:

$$\mu = \tan\varphi \tag{4.1}$$

Using estimated value of 0.37 for the friction coefficient, internal friction angle for the soft sandstone turns out to be 20.30 degrees.

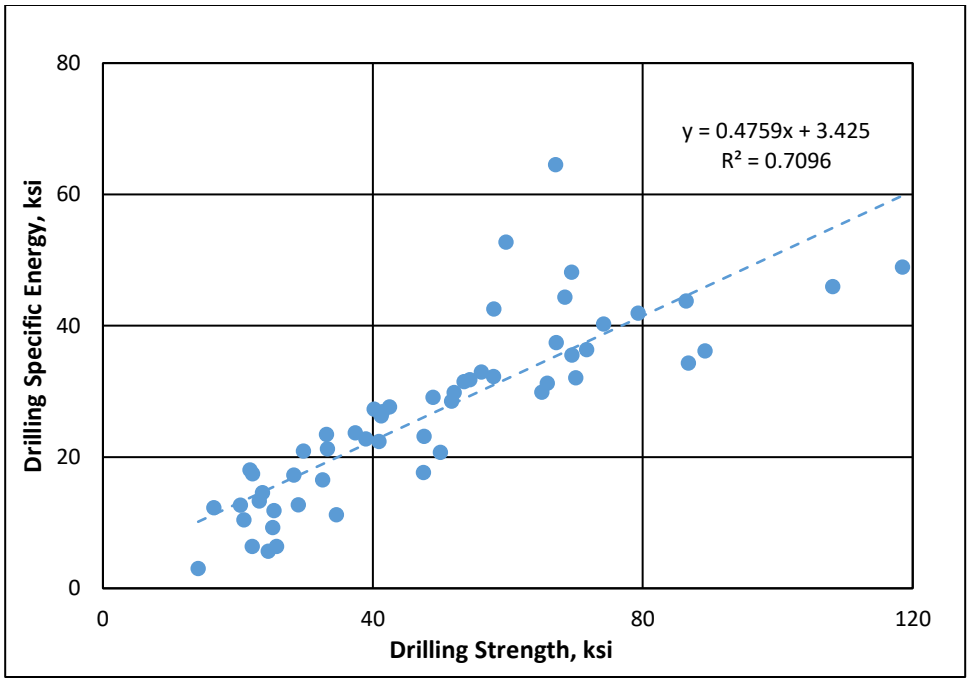

Figure 4.14: E-S plot for experimental data

4.3 Lateral Vibrations

Hard Sandstone: Figure 4.15 mostly shows a gradual increase of lateral vibrations with rotational speed at constant WOB. At high WOB (37.52 lbf), the vibration increased sharply with the speed. Similar experiment was performed by Mihajlovic et al. (2007) as discussed in Section 2.3. In Fig. 4.16, line e4 represents the equilibrium line with no torsional vibrations. The measurements show similar lateral vibration trend with rotational speed.

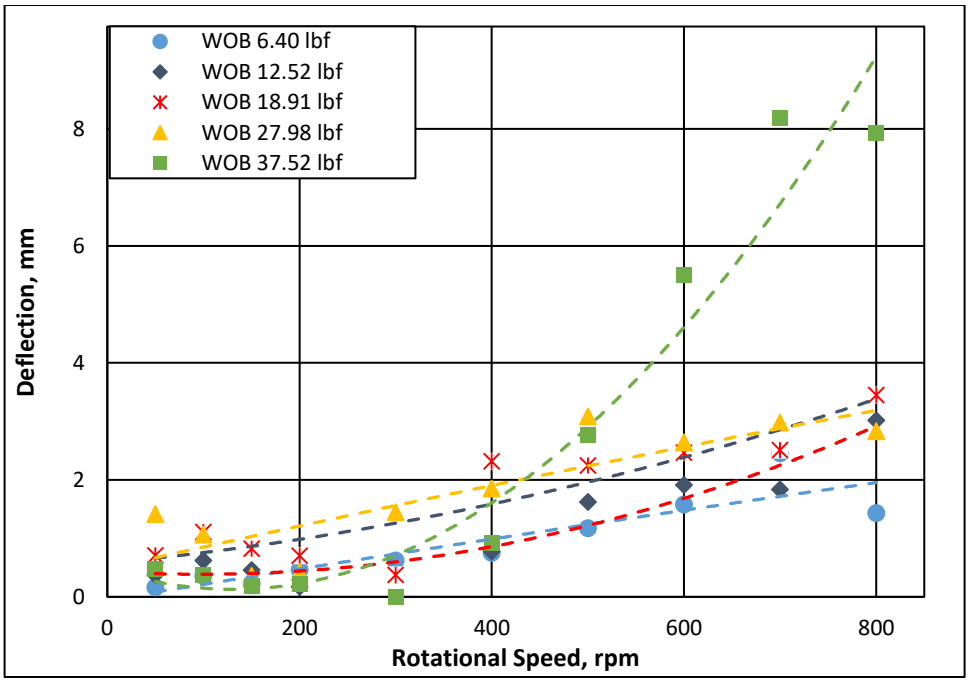

Figure 4.15: Lateral vibration vs. rotational speed (hard sandstone)

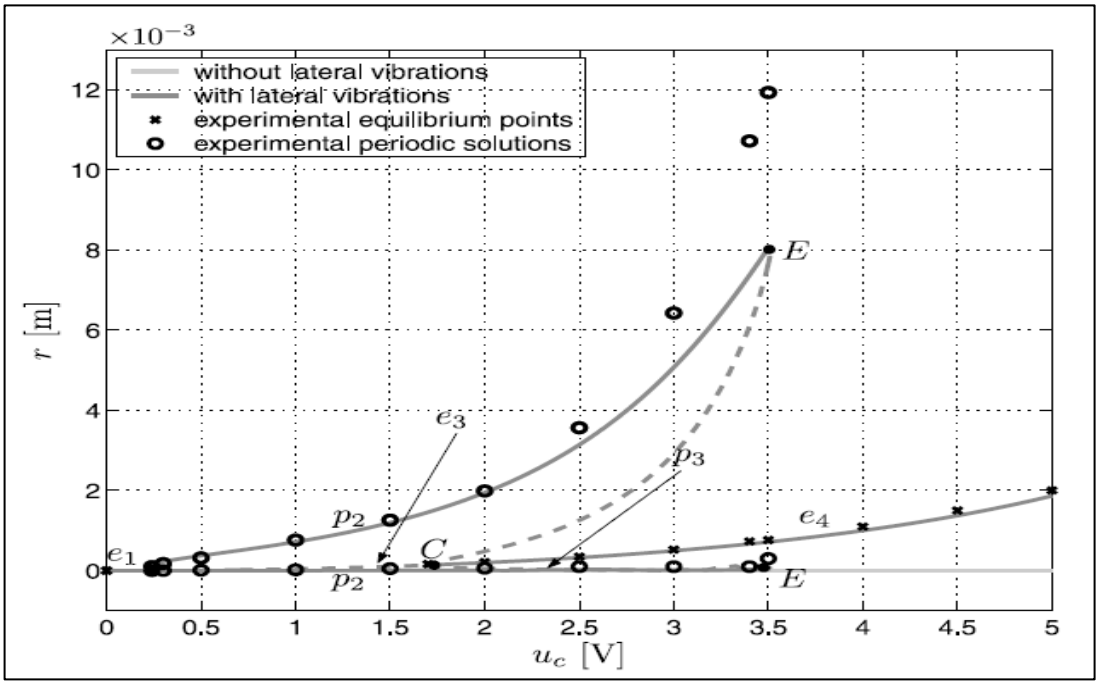

Figure 4.16: Radial displacement of lower disc vs topdrive voltage (Mihajlovic et al. 2007)

At low rotational speeds (less than 500 rpm), lateral vibration increased at low WOBs (Fig. 4.17). Its trend changed at high WOB. The decrease can be attributed to

the bowing of the drillstring at higher WOB inducing greater amplitude of displacement towards the sensor.

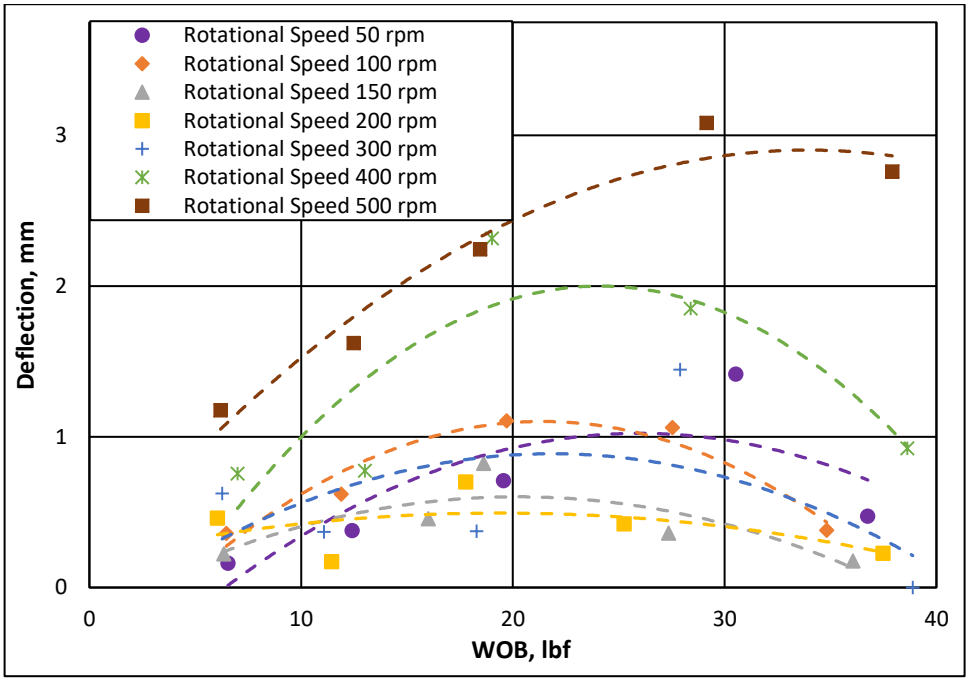

Figure 4.17: Lateral vibration vs. WOB (hard sandstone)

At high rotational speeds (greater than 600 rpm), the lateral vibration trend with WOB was predominantly increasing (Fig. 4.18). It can be hypothesized that at higher RPM the centrifugal force on the drillstring increased, which along with impact load from the casing shoe walls induced bowing in opposite direction resulting in excessive deflection away from the sensor. Hard sandstone induced excessive vibrations which reversed the bowing tendency. Such a trend is not observed during soft sandstone test.

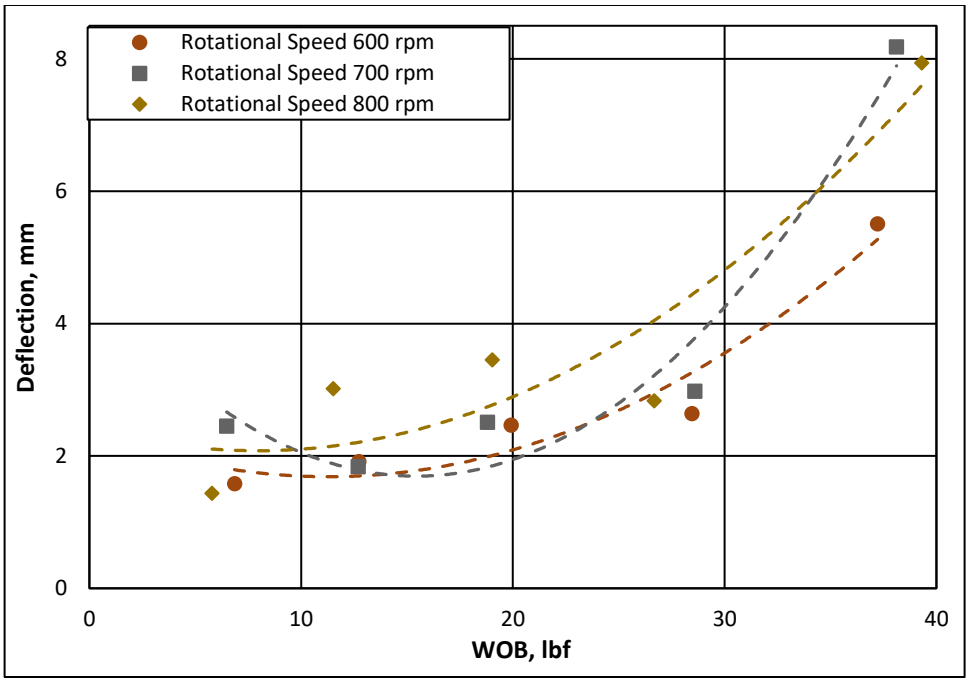

Figure 4.18: Lateral vibration vs. WOB (hard sandstone)

Soft sandstone: There is a general trend of increase in lateral vibration with rotational speed (Fig. 4.19), even though it is not as significant as in hard sandstone. Despite significant scattering of the data, trendlines from the measurements predominantly show a general trend of increase in lateral vibrations with WOB at low WOBs and trend reversal at high WOBs (Figs. 4.20 and 4.21). The trend reversal at higher WOB shows a decrease in deflection amplitude. This can be attributed to the bending of the pipe due to higher axial load, which makes the pipe to bend more on the sensor side causing reduction in the deflection.

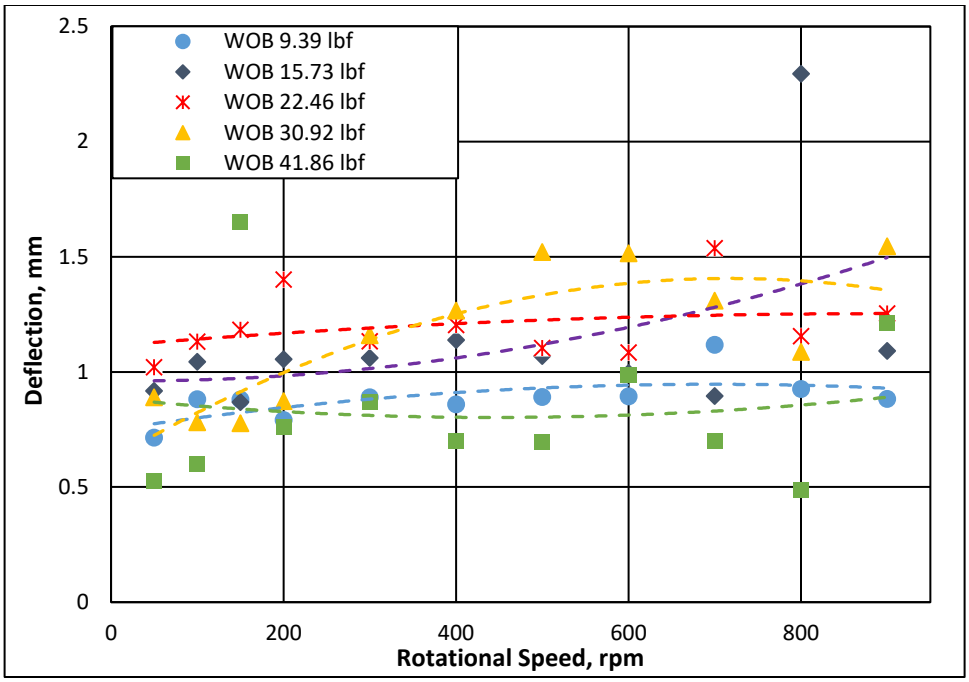

Figure 4.19: Lateral vibration vs. rotational speed (soft sandstone)

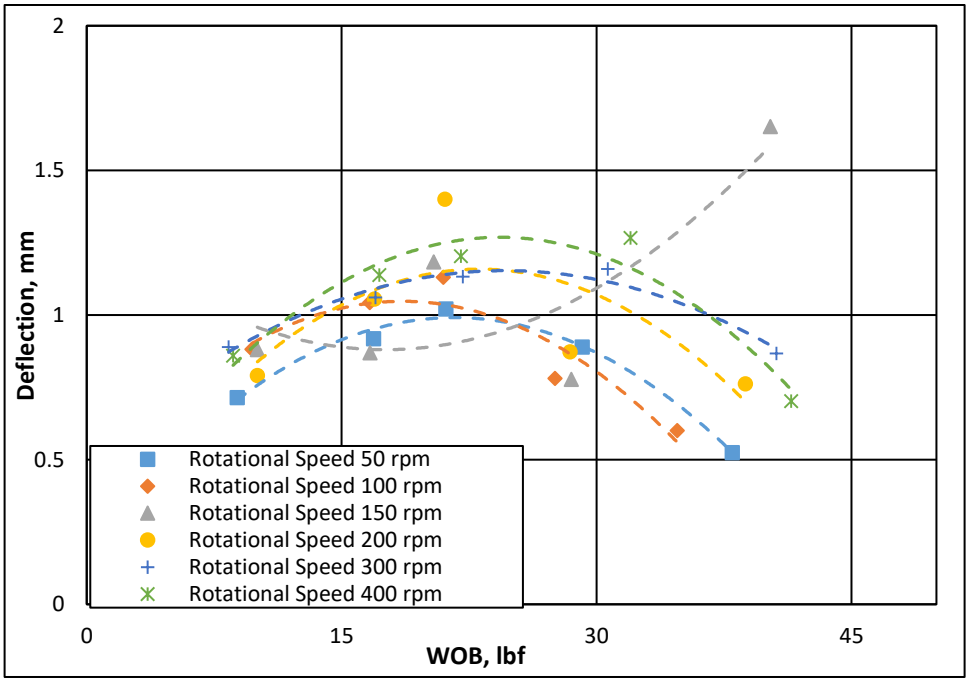

Figure 4.20: Lateral vibration vs. WOB (soft sandstone)

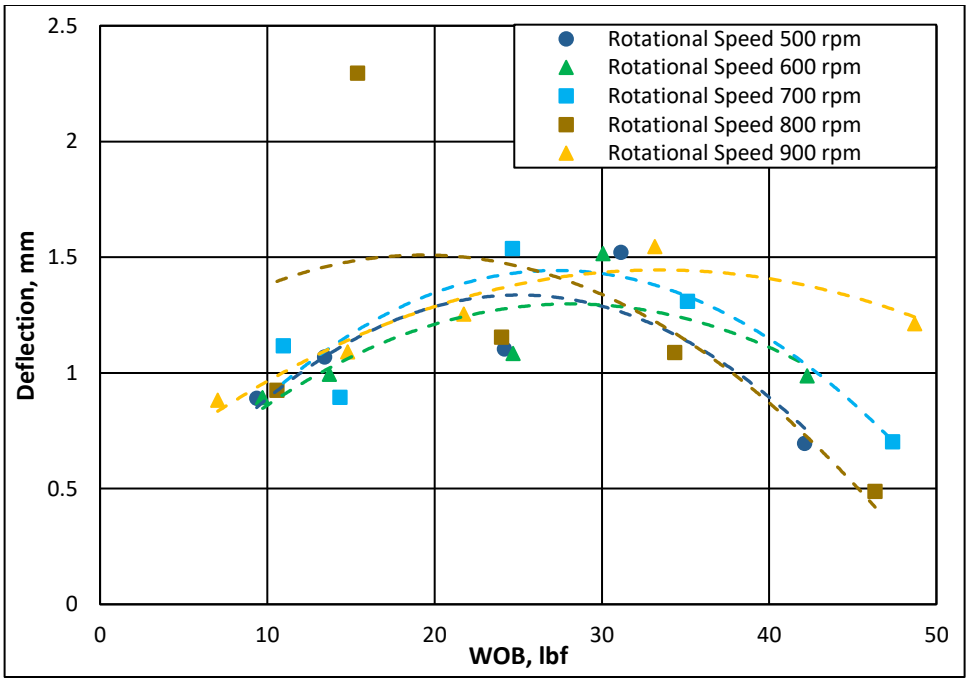

Figure 4.21: Lateral vibration vs. WOB (soft sandstone)

4.4 Axial Vibrations

Hard Sandstone: Axial vibration exhibited slightly different trend from lateral vibration (Fig. 4.22). With an increase in speed, axial vibration increased significantly. However, the gradient diminished as the speed was increased and eventually reaching to a turning point for most of the measurements. Similar to the trend for torque (Fig. 4.1), some cases have abnormally high vibration magnitude at 200 and 300 rpm which can be attributed to abnormally hard layer of formation. Finnie and Bailey (1960) observed that torque was coupled with axial vibration during field measurements.

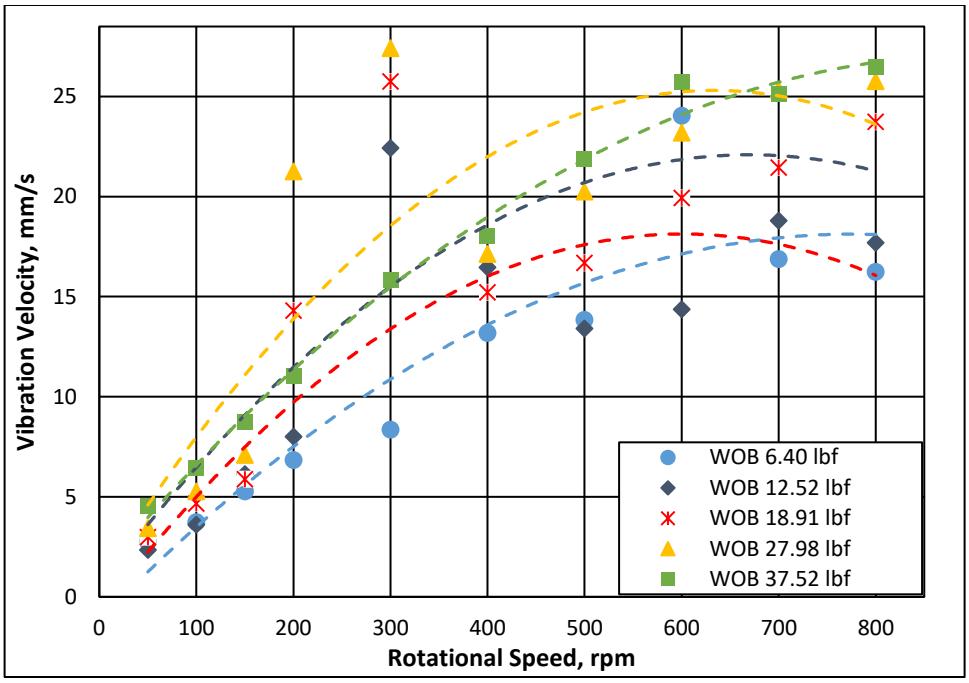

Figure 4.22: Axial vibration vs. rotational speed (hard sandstone)

Figure 4.23 shows vibration severity as per ISO 10816-1:1995 which classifies mechanical vibration of machines by measurement of vibration on non-rotating parts. As the rig operates at low power (less than 15 kW), it is classified in Class 1 small machines. As can be seen from the standard, vibration velocity greater than 7.10 mm/s is extremely harmful to the machinery. The plots for hard sandstone (Fig. 4.25) shows higher rotational speed than 150 rpm generating vibration magnitude high enough to cause damage to the machinery. Similar results were obtained by Esmaeili et al. (2012), who recommended the range of 100 - 120 rpm as optimum operating range (Fig. 4.24). Vibration amplitude increased with rotational speed and WOB.

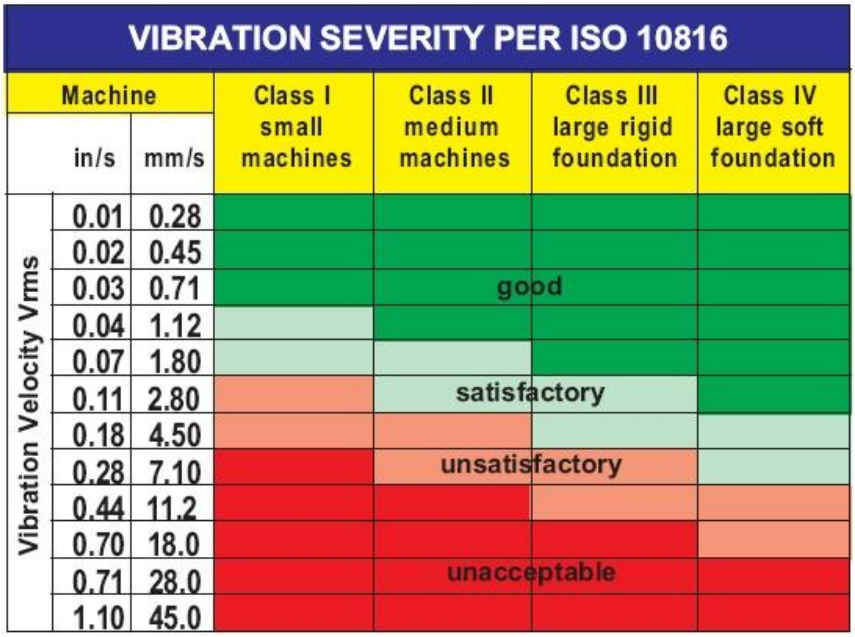

Figure 4.23: Vibration severity standard as per ISO 10816 (Reliability Direct)

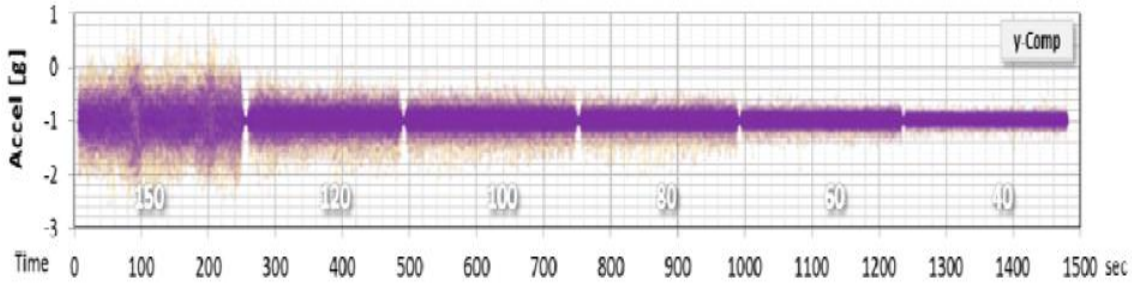

Figure 4.24: Axial vibration data at 800 N WOB and rotational speed from 40 to 120 rpm (Esmaeili et al. 2012)

The trend of axial vibrations with WOB varies with the speed range (Figs. 4.25 and 4.26). At intermediate rotational speeds (200 and 300 rpm), the vibration increased with WOB when WOB was maintained approximately less than 22.5 lbf. At higher WOB, trend reversal was observed. This trend was not observed in other speeds. At constant rotational speed, the vibration predominantly increased with WOB. As discussed previously, it can be observed that vibration at 200 and 300 rpm are

significantly higher than that of other speeds in the same range. Vibration magnitudes of these speeds are similar to that of 700 and 800 rpm. No such phenomenon was observed with soft sandstone (Fig. 4.27). Therefore, it can be concluded that the unusual high axial vibration is observed due to non-conformity of the rock sample.

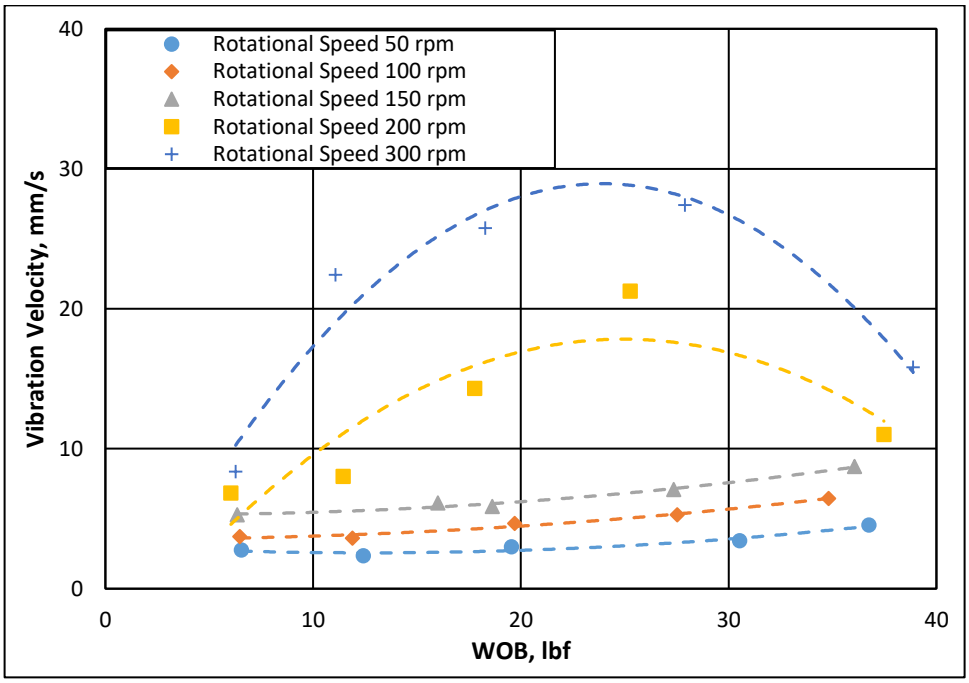

Figure 4.25: Axial vibration vs. WOB (hard sandstone)

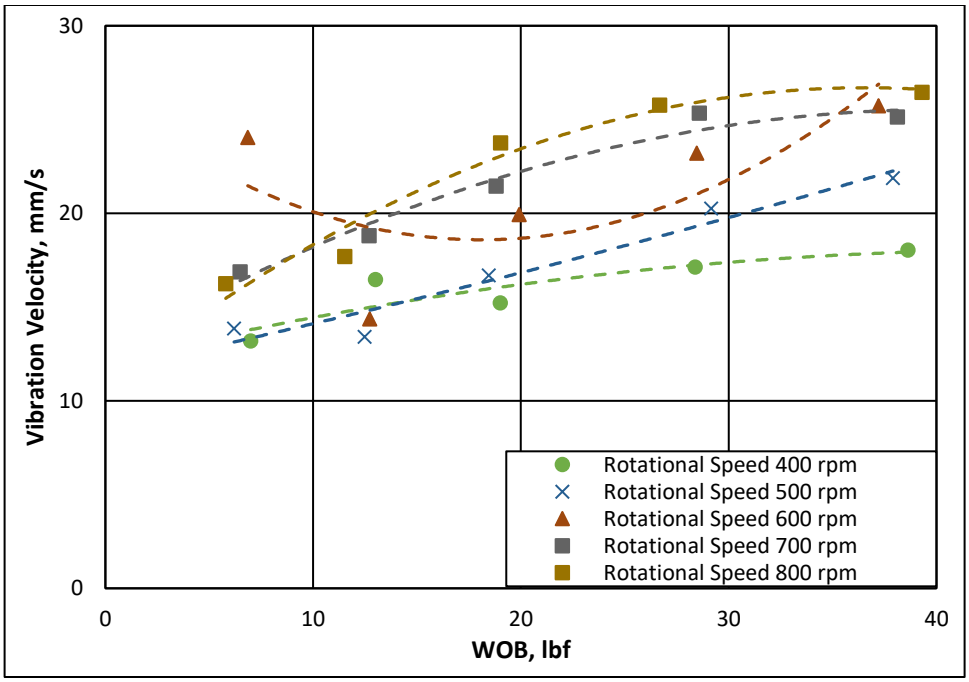

Figure 4.26: Axial vibration vs. WOB (hard sandstone)

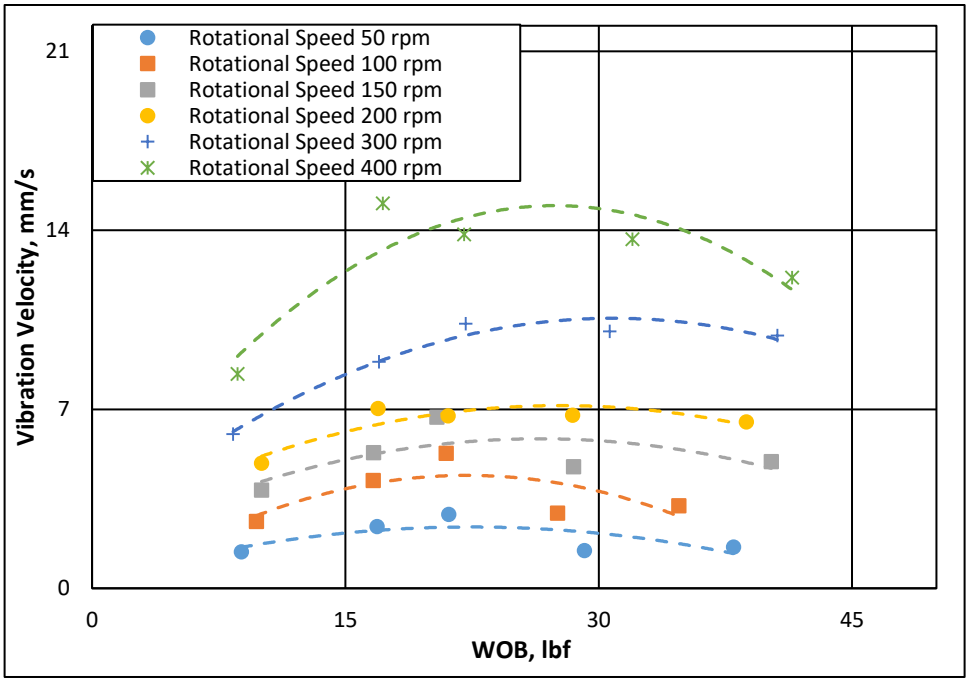

Figure 4.27: Axial vibration vs. WOB (soft sandstone)

Soft sandstone: For hard sandstone, with increase in rotational speed, axial vibration increased (Fig. 4.22). However, the gradient gradually diminished when the speed was increased reaching to a turning point for most of the data. The vibration trend of the soft sandstone (4.28) resembles to that of the hard sandstone.

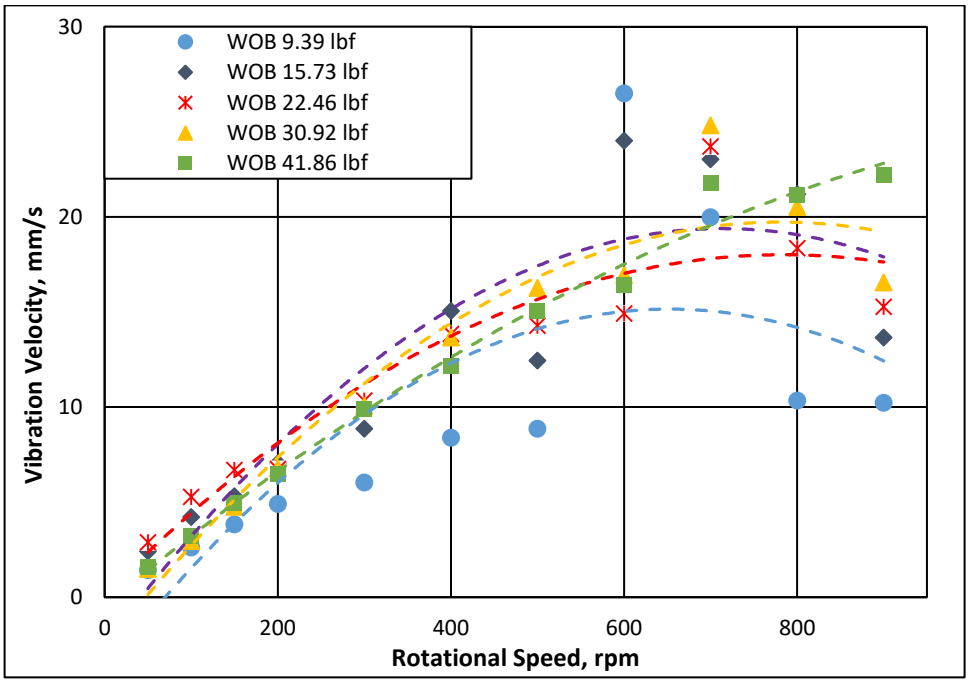

Figure 4.28: Axial vibration vs. rotational speed (soft sandstone)

There is a sudden increase in axial vibration at 700 rpm and then gradual reduction. This occurrence can be attributed to the phenomenon of resonance. Daering and Livesay (1968) observed severe axial vibration at certain critical speeds. Based on the modal analysis (Table 4.2) performed in ANSYS for the aluminum drillstring, it was found that natural frequency of the pipe is 10.37 Hz (622 rpm). With the support from the walls and the attached bit and bit sub, it can be assumed that the first mode shifted

from 622 rpm to somewhere around 700 rpm. Due to resonance, the vibration frequency increases which is the reason for sudden increase in axial vibration at 700 rpm.

Table 4.2: Result of modal analysis for drillstring and bit sub

Mode	Drillstring Frequency [Hz]	Bit Sub Frequency [Hz]
1	10.37	2808.6
2	10.37	2808.6
3	64.93	10270
4		11600
5	181.55	11646
6		12722

The general axial vibration trend with WOB is mostly increasing at low WOBs and trend reversal at high WOB (Figs. 4.27 and 4.29). However, there are some exceptions (600 and 900 rpm) that do not follow this trend. For soft sandstone, the threshold rpm according to the vibration severity standard is around 200 rpm which is 50 rpm higher than that of hard sandstone. This suggests that the hardness of the rock being cut influences axial vibration.

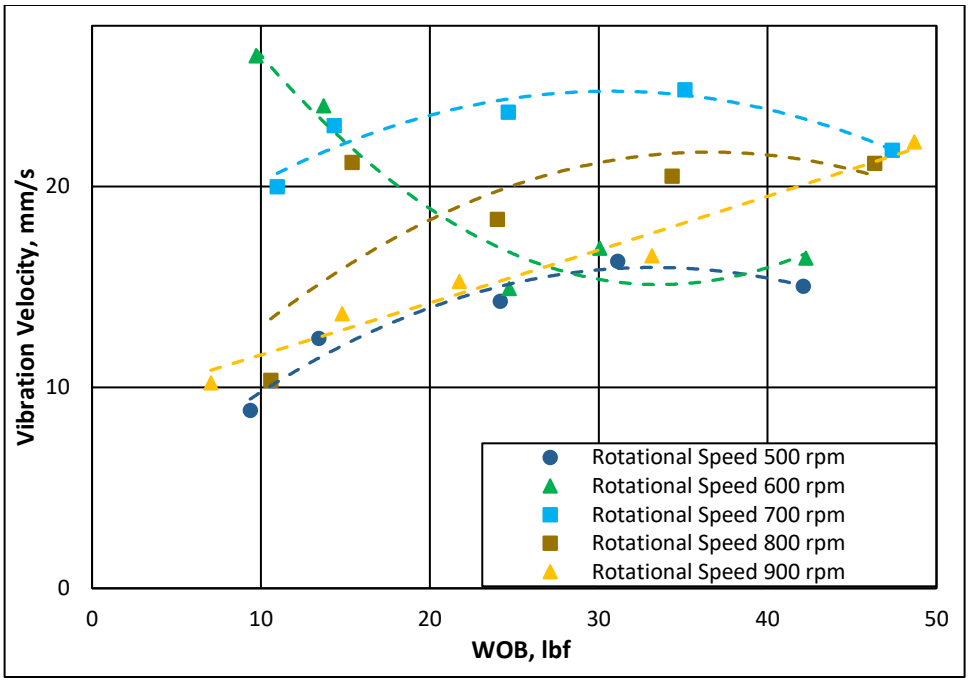

Figure 4.29: Axial vibration vs. WOB (soft sandstone)

4.5 Effect on ROP

The hard sandstone had extremely small drilled depth which was undetectable by the displacement sensor. Hence the ROP measurements could not be obtained for analysis. Measurements obtained from soft sandstone are compared with published data (Esmaeili et al. 2012) generated using roller cone bit (Fig. 4.30). Measured ROP increases with rotational speed at constant WOB (Fig. 4.31). ROP peaks at around 700 rpm and then it decreases. This can be attributed to the percussive drilling action. From axial vibration plot (Fig. 4.28) it can be observed that ROP follows the axial vibration trend. The hammering action helps destress the rock formation and provide ease in drilling. The measured ROP trend is consistent with a typical ROP versus rotational speed plot (Fig. 4.32). The decline from point b to c is attributed to poor hole cleaning.

In this study, the rotational speed above 700 rpm was too high exciting vibration such that the bit was sliding over the rock and it did not have enough weight to push it down and provide a depth of cut. When the WOB was high (around 37 pounds), the ROP increased as the force kept the bit in contact with the rock, supporting the previous hypothesis.

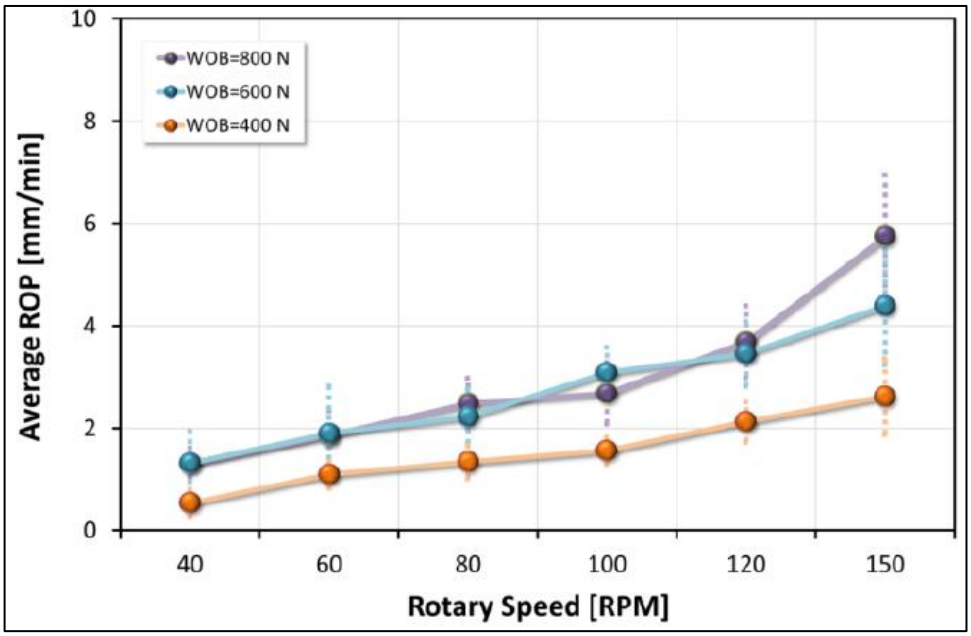

Figure 4.30: ROP vs rotational speed using a dual cone bit (Esmaeili et al. 2012)

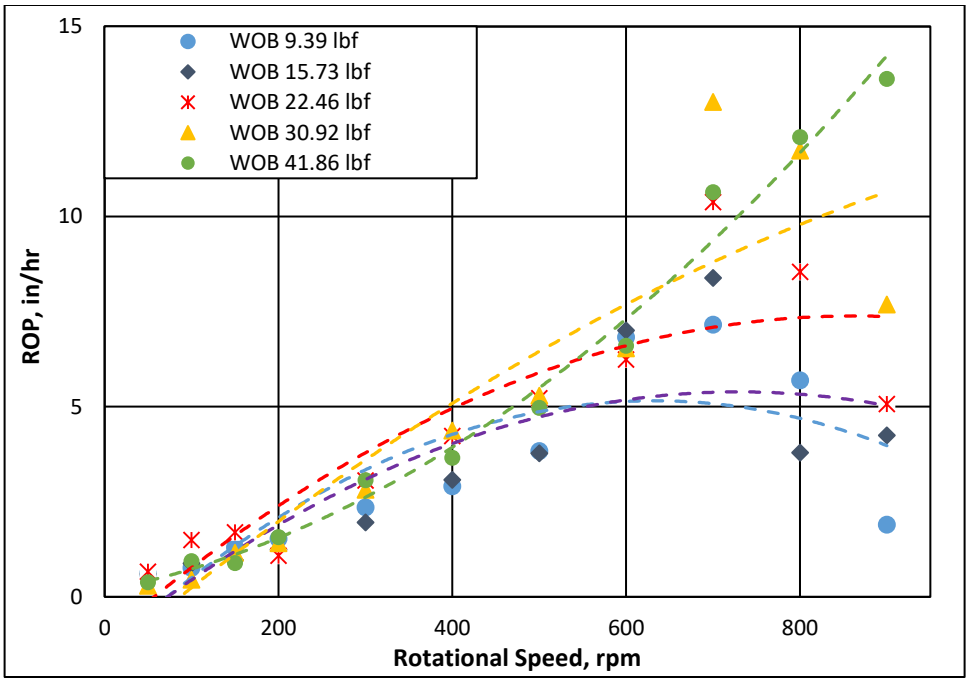

Figure 4.31: ROP vs. rotational speed (soft sandstone)

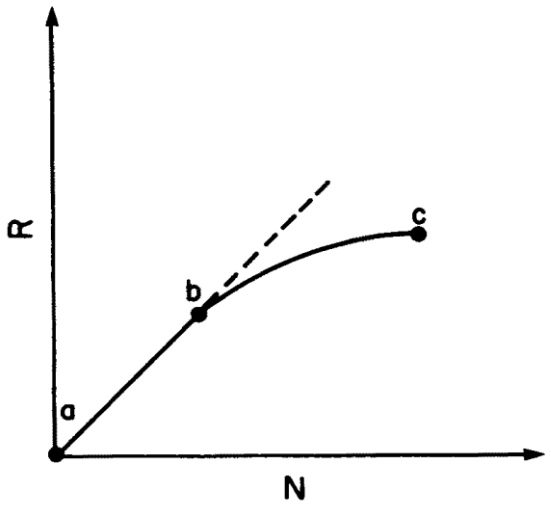

Figure 4.32: General trend for ROP vs rotational speed graph (Bourgoyne et al. 1986)

5. CONCLUSIONS AND RECOMMENDATIONS

5.1 Conclusions

An automated rig has been constructed and a total of 105 experiments were performed on 2 different rock samples. Based on the interpretations of the data obtained from experiments and comparison with the torque model following can be concluded:

- Analytical bit rock interaction model proposed by Detournay and Defourny reasonably describes the relationship between rotational speed, WOB, ROP and depth of cut, when model parameters are systematically selected.
- Bit constant is an important parameter for the analytical model. The distribution of cutting forces depends on the bit constant and may provide inaccurate results if not estimated correctly. The estimated value of bit constant is lower at low WOB.
- The assumed value of intrinsic specific energy of the sample sandstone is different than that of Berea sandstone. Friction coefficient between sample sandstone and carbide cutter is approximately 0.37 with lubrication provided by water.
- At constant WOB, with increase in rotational speed, increase in lateral vibrations in hard sandstone is higher than in soft sandstone which indicates that lateral vibrations also depend on type of formation.
- Axial vibrations are coupled with torque. With change in torque, a corresponding change in axial vibrations is observed. The axial vibrations above 150 rpm are damaging to the drillstring and experimental setup.

- WOB has less effect on excitation of axial vibration in soft rocks than hard rocks. Hence the set-point WOB should be decreased when drilling into hard rocks.
- Effect of rotational speed on axial vibrations is greater than that of WOB. Hence, in case of decreasing axial vibrations, decrease in rotational speed will lead to better control of axial vibrations.
- Rotational speed of 700 rpm is the highest rotational speed which can be used to obtain highest ROP without taking the increased vibrations into account. Increase of rotational speed further lowers the ROP due to reduction of contact time between the bit and rock surface.

5.2 Recommendations and Future Work

Although the design of the rig was optimized, there is always room for improvement. With an increase in budget and limited design constraints, the rig can be constructed better. Following are the recommendations for upgrading the rig.

- The software program used for the control algorithm can be upgraded to more user-friendly software for programming the automation and control architecture.
- A vibrating element can be attached to the travelling block when WOB calibration is performed so that error due to change in friction values can be minimized.
- The spring couplings attached to the torque sensor can be upgraded with a higher torque rating to prevent failure at higher vibrations.
- A stable support structure for the torque sensor and laser deflection sensor can be provided.

A set of experiments could be designed where bit geometry, cutter density and cutter size could be varied to obtain a relationship between these bit parameters to obtain bit constant.

Forward and backward whirl characterization experiments could be performed with sensors capable of detecting whirl rates.

Hammering action can be included in the drilling action and its coupled effect on ROP, lateral vibrations, torque and axial vibrations could be analyzed.

Nomenclature

Symbols

a	Bit Radius, in
A	Cross-sectional area of cut, in^2
A_t	Area of nozzles, in^2
C_d	Coefficient of discharge
E	Drilling Specific Energy, psi
E_x	Modulus of elasticity, psi
F_b	Buckling force, lbf
F_j	Jet Impact Force, lbf
I	Area Moment of Inertia, in^4
K	Column effective length
L	Length of drill pipe,
OD	Outer Diameter, in
P	Burst pressure, psi
q	Flowrate, gpm
S	Drilling Strength, psi
T	Torque, in-lbf
t	Drill pipe thickness, in
T_c	Cutting component of torque
T_f	Friction component of torque
T_{max}	Maximum torque, in-lbf
UCS	Unconfined Compressive Strength

W_c	Cutting component of WOB
W_f	Frictional component of WOB
WOB, W	Weight on Bit, lbf
Y	Minimum Yield Strength, psi
ΔP_b	Pressure drop across bit nozzles, psi

Greek Symbols

μ	Friction coefficient of wearflat
γ	Bit constant
δ	Depth of cut per revolution, in/rpm
ϵ	Intrinsic Specific Energy, psi
ζ	Drilling strength to rock strength ratio
ρ	Density of water, ppg
σ_{max}	Maximum shear strength, psi

Acronyms

BHA	Bottom Hole Assembly
DSATS	Drilling Systems Automation and Technical Section
FEM	Finite Element Method
gpm	Gallons Per Minute
MWD	Measurement While Drilling
PDC	Polycrystalline Diamond Compact
psi	Pound per square inch

ROP, v	Rate of Penetration, ft/hr
rpm, ω	Rotation Per Minute
SPE	Society of Petroleum Engineers
VBA	Visual Basic for Applications

References

Bailey, J. J. and Finnie, I. 1960. An Analytical Study of Drill-String Vibration. *ASME Journal of Engineering for Industry* 82 (2): 122-127. http://dx.doi.org/10.1115/1.3663017.

Bailey, J. R., Biediger, E., Sundararaman, S. et al. 2008. Development and Application of a BHA Vibrations Model. International Petroleum Technology Conference, Kuala Lumpur, Malaysia, 3-5 December. IPTC-12737-MS. https://doi.org/10.2523/IPTC-12737-MS.

Baumgart, A. 2000. Stick-Slip and Bit-Bounce of Deep-Hole Drillstrings. *Transactions-American Society of Mechanical Engineers Journal of Energy Resources Technology* 122 (2): 78-82. http://dx.doi.org/10.1115/1.483168.

Bavadiya, V. A., Aljubran, M. J., Kibe, J. M. et al. 2015. Design, Construction and Operation of an Automated Drilling Rig for the DSATS University Competition. SPE Annual Technical Conference and Exhibition, Houston, Texas, 28-30 September. SPE-174920-MS. http://dx.doi.org/10.2118/174920-MS.

Berlioz, A., Der Hagopian, J., Dufour, R. et al. 1996. Dynamic Behavior of a Drill-string: Experimental Investigation of Lateral Instabilities. *Journal of Vibration and Acoustics* **118** (3): 292-298. http://dx.doi.org/ 10.1115/1.2888180.

Black, A.D., Walker, B.H., Tibbitts, G.A. et al. 1986. PDC Bit Performance for Rotary, Mud Motor, and Turbine Drilling Applications. *SPE Drilling Engineering* **1** (06): 409-416. SPE-13258-PA. https://dx.doi.org/10.2118/13258-PA.

Bourgoyne, A.T., Millheim, K.K., Chenevert, M.E. and Young, F.S. 1986. *Applied Drilling Engineering*, 1st ed. Richardson, Texas: The Society of Petroleum Engineers.

Brett, J. F. (1992). The Genesis of Torsional Drillstring Vibrations. *SPE Drilling Engineering* **7** (3): 168–174. SPE-21942-PA. http://dx.doi.org/10.2118/21943-PA.

Challamel, N., Sellami, H., Chenevez, E. et al. 2000. A Stick-slip Analysis Based on Rock/Bit Interaction: Theoretical and Experimental Contribution. IADC/SPE Drilling Conference, New Orleans, Louisiana, 23-25 February. SPE-59230-MS. http://dx.doi.org/10.2118/59230-MS.

Chen, S.L. and Géradin, M. 1995. An Improved Transfer Matrix Technique as Applied to BHA Lateral Vibration Analysis. *Journal of Sound and Vibration* **185** (1): 93-106. https://dx.doi.org/10.1006/jsvi.1994.0365.

Cheng, L., Tianhuai, D., and Peng, W. 2011. An experimental rig for near-bit force measurement and drillstring acoustic transmission of BHA. *Measurement* **44** (4): 642-652. http://dx.doi.org/10.1016/j.measurement.2010.12.005.

Chin, W.C., 2014. Wave Propagation in Drilling, Well Logging and Reservoir Applications. Massachusetts, Scrivener.

Christoforou, A. P. & Yigit, A. S. 2001. Active Control of Stick-Slip Vibrations: The Role of Fully Coupled Dynamics. SPE Middle East Oil Show, Manama, Bahrain, 17-20 March. SPE-68093-MS. http://dx.doi.org/10.2118/68093-MS.

Dareing, D. W. 1984. Drill Collar Length is a Major Factor in Vibration Control. *Journal of Petroleum Technology* **36** (04): 637-644. SPE-11228-PA. http://dx.doi.org/10.2118/11228-PA.

Dareing, D. W. 1985. Vibrations Increase Available Power at the Bit. *ASME Journal of Energy Resources Technology* **107** (1): 138-141. http://dx.doi.org/10.1115/1.3231153.

Dareing, D. W. and Livesay B. J. 1968. Longitudinal and Angular Drill-String Vibrations with Damping. *ASME Journal of Engineering for Industry* **90**(4): 671-679. http://dx.doi.org/10.1115/1.3604707.

Detournay, E. and Defourny, P. 1992. A Phenomenological Model for the Drilling Action of Drag Bits. *International Journal of Rock Mechanics and Mining Sciences and Geomechanics Abstracts* **29** (1): 13-23. https://doi.org/10.1016/0148-9062(92)91041-3.

Dykstra, M. W., Chen, D. K., and Warren, T. M. 1994. Experimental evaluations of drill bit and drill string dynamics. SPE Annual Technical Conference and Exhibition, New Orleans, Louisiana, 25-28 September. SPE-28323-MS. https://dx.doi.org/10.2118/28323-MS.

Dykstra, M. W., Chen, D. K., Warren, T. M. et al. 1996. Drillstring Component Mass Imbalance: A Major Source of Downhole Vibrations. *SPE Drilling and Completion* **11** (04): 171-178. PE-29350-PA. http://dx.doi.org/10.2118/29350-PA.

Esmaeili, A., Elahifar, B., Fruhwirth, R. K. et al. 2012. Laboratory Scale Control of Drilling Parameters to Enhance Rate of Penetration and Reduce Drill String

Vibration. SPE Saudi Arabia Section Technical Symposium and Exhibition, Al-Khobar, Saudi Arabia, 8-11 April. SPE-160872-MS. http://dx.doi.org/10.2118/160872-MS.

Finnie, I. and Bailey, J. J. 1960. An Experimental Study of Drill-String Vibrations. *Journal of Engineering for Industry* **82** (2): 129-135. http://dx.doi.org/10.1115/1.3663020.

Forster, I. 2011. Axial Excitation as a Means of Stick Slip Mitigation-Small Scale Rig Testing and Full Scale Field Testing. SPE/IADC Drilling Conference and Exhibition, Amsterdam Netherlands, 1-3 March. SPE-139830-MS. https://dx.doi.org/10.2118/139830-MS.

Forster, I., Macfarlane, A.H.W., and Dinnie, R. 2010. Asymmetric Vibration Damping Tool--Small Scale Rig Testing and Full Scale Field Testing. IADC/SPE Drilling Conference and Exhibition, New Orleans, Louisiana, 2-4 February. SPE-128458-MS. https://doi.org/10.2118/128458-MS.

Franca, F. P. 2010. Drilling Action of Roller-Cone Bits: Modeling and Experimental Validation. *Journal of Energy Resources Technology* **132** (4): 043101. http://dx.doi.org/ doi:10.1115/1.4003168.

Freudenrich, C. and Strickland, J. 2001 How Oil Drilling Works. How Stuff Works, http://science.howstuffworks.com/environmental/energy/oil-drilling4.htm (10 March 2017).

Glowka, D. A. 1989. Use of Single-Cutter Data in the Analysis of PDC Bit Designs: Part 1 - Development of a PDC Cutting Force Model. *SPE Journal of Petroleum*

Technology **41** (08): 797-849. SPE-15619-PA. https://dx.doi.org/10.2118/15619-PA.

Gulyaev, V. I., Lugovoi, P. Z., Belova, M. A. et al. 2006. Stability of the equilibrium of rotating drillstrings. *International Applied Mechanics* **42**: 692. http://dx.doi.org/10.1007/s10778-006-0137-5.

Halsey, G. W., Kyllingstad, A., Aarrestad, T. V. et al. 1986. Drillstring Torsional Vibrations: Comparison Between Theory and Experiment on a Full-Scale Research Drilling Rig. SPE Annual Technical Conference and Exhibition, New Orleans, Louisiana, 5-8 October. SPE-15564-MS. http://dx.doi.org/10.2118/15564-MS.

Jain, J. R., Ledgerwood, L. W., Hoffmann, O. J. M. et al. 2011. Mitigation of Torsional Stick-Slip Vibrations in Oil Well Drilling through PDC Bit Design: Putting Theories to the Test. SPE Annual Technical Conference and Exhibition, Denver Colorado, 30 October-2 November. SPE-146561-MS. http://dx.doi.org/10.2118/146561-MS.

Jansen, J. D. 1991. Non-linear Rotor Dynamics as Applied to Oilwell Drillstring Vibrations. *Journal of Sound and Vibration* **147** (1): 115-135. https://dx.doi.org/10.1016/0022-460X(91)90687-F.

Jansen, J. D. and Van Den Steen, L. 1995. Active Damping of Self-Excited Torsional Vibrations in Oil Well Drillstrings. *Journal of Sound and Vibration* **179** (4): 647–668. https://dx.doi.org/10.1006/jsvi.1995.0042.

Jogi, P. N., Macpherson, J. D., and Neubert, M. 2002. Field verification of model-derived natural frequencies of a drill string. *ASME Journal of Energy Resources Technology*, **124** (3): 154-162. http://dx.doi/10.1115/1.1486018.

Khulief, Y. A. and Al-Naser, H. 2005. Finite Element Dynamic Analysis of Drillstrings. *Finite Elements in Analysis and Design* **41** (13): 1270-1288. http://doi.org/10.1016/j.finel.2005.02.003.

Khulief, Y.A. and Al-Sulaiman, F.A., 2009. Laboratory Investigation of Drillstring Vibrations. Proceedings of the Institution of Mechanical Engineers, Part C: *Journal of Mechanical Engineering Science* **223** (10): 2249-2262. https://dx.doi.org/10.1243/09544062JMES1550.

Li, Z. and Guo, B. 2007. Analysis of Longitudinal Vibration of Drill String in Air and Gas Drilling. Rocky Mountain Oil and Gas Technology Symposium, Denver, Colorado, 16-18 April. SPE-107697-MS. http://dx.doi.org/10.2118/107697-MS.

Lin, Y. Q. and Wang, Y. H. 1991. Stick-Slip Vibration of Drill Strings. *Journal of Engineering for Industry* 113 (1): 38-43. http://dx.doi.org/10.1115/1.2899620.

Lu, H., Dumon, J., and Canudas de Wit, C. 2009. Experimental study of the D-OSKIL mechanism for controlling the stick-slip oscillations in a drilling laboratory testbed. IEEE Multi-conference on Systems and Control, Jul 2009, Saint Petersburg, Russia. HAL Id: hal-00385549, version 1.

Macpherson, J. D., Jogi, P. N., and Vos, B. E. 2001. Measurement of Mud Motor Rotation Rates using Drilling Dynamics. SPE/IADC Drilling Conference, Amsterdam, Netherlands, 27 February-1 March. SPE-67719-MS. http://dx.doi.org/10.2118/67719-MS.

Melakhessou, H., Berlioz, A., and Ferraris, G. 2003. A Nonlinear Well-Drillstring Interaction Model. *ASME Journal of Vibration and Acoustics* **125** (1): 46–52. http://dx.doi.org/10.1115/1.1523071.

Mihajlović, N., Wouw, N.V.D., and Rosielle, P.C. et al. 2007. Interaction Between Torsional and Lateral Vibrations in Flexible Rotor Systems with Discontinuous Friction. *Nonlinear Dynamics* **50** (3): 679-699. http://dx.doi.org/10.1007/s11071-006-9172-3.

Mitchell, R. F. and Allen, M. B. 1987. Case Studies of BHA Vibration Failure. SPE Annual Technical Conference and Exhibition, Dallas, Texas, 27-30 September. SPE-16675-MS. https://dx.doi.org/10.2118/16675-MS.

Paslay, P. R. and Bogy, D. B. 1963. Drill String Vibrations Due to Intermittent Contact of Bit Teeth. *ASME. Journal of Engineering for Industry* **85** (2): 187-194. http://dx.doi.org/10.1115/1.3667632.

Patil, P. A. and Teodoriu, C., 2013a. Model Development of Torsional Drillstring and Investigating Parametrically the Stick-Slips Influencing Factors. *Journal of Energy Resources Technology* **135** (1): 013103. JERT-12-1158. http://dx.doi.org/ 10.1115/1.4007915.

Patil, P. A. and Teodoriu, C., 2013b. A Comparative Review of Modelling and Controlling Torsional Vibrations and Experimentation Using Laboratory Setups. *Journal of Petroleum Science and Engineering* **112**: 227-238. http://dx.doi.org/10.1016/j.petrol.2013.11.008.

Raymond, D. W., Elsayed, M. A., Polsky, Y. et al. 2008. Laboratory Simulation of Drill Bit Dynamics Using a Model-Based Servohydraulic Controller. *ASME Journal*

of Energy Resources Technology **130** (4): 043103-12. http://dx.doi.org/10.1115/1.3000142.

Richard, T., Germay, C. and Detournay, E., 2007. A Simplified Model to Explore the Root Cause of Stick–Slip Vibrations in Drilling Systems with Drag Bits. *Journal of Sound and Vibration* **305** (3): 432-456. http://doi.org.ezproxy.lib.ou.edu/10.1016/j.jsv.2007.04.015.

Schlumberger Educational Services. 2004. Powerpak Steerable Motor Handbook. Schlumberger Drilling and Measurements, Sugarland , Texas.

Swenson, D. V., Wesenberg, D. L., and Jones, A. K. 1981. Analytical and Experimental Investigations of Rock Cutting Using Polycrystalline Diamond Compact Drag Cutters. SPE Annual Technical Conference and Exhibition, San Antonio, Texas, 4-7 October. SPE-10150-MS. http://dx.doi.org/10.2118/10150-MS.

Tingey, D. 2015. Design, Fabrication and Preliminary Testing of Experimental Rock Drilling Rig. MS Thesis, Texas A&M University, College Station, Texas, USA (August 2015). http://hdl.handle.net/1969.1/155733.

Tucker, R. W. and Wang, C. 2000. The Excitation and Control of Torsional Slip-Stick in the Presence of Axial Vibrations. Citeseer Computer and Information Science Publications Collection. Id: 41923656.

Vandiver, J. K., Nicholson, J. W., and Shyu, R. J. 1990. Case Studies of the Bending Vibration and Whirling Motion of Drill Collars. *SPE Drilling Engineering* **5** (04): 282-290. SPE-18652-MS. https://doi.org/10.2118/18652-PA.

Vibration Severity Standards ISO 10816 http://www.reliabilitydirectstore.com/v/vspfiles/RDIStorePDF/VibrationChart.pdf (accessed 10 March 2017).

Wilson, J. K. 2013. Design and Analysis of a Test Rig for Modeling the Bit/Formation Interface in Petroleum Drilling Applications. MS Thesis, Texas A&M University, College Station, Texas, USA (May 2013). http://hdl.handle.net/1969.1/149457.

Wojtanowicz, A. K. and Kuru, E. E. 1993. Mathematical Modeling of PDC Bit Drilling Process Based on a Single-Cutter Mechanics. *ASME. Journal of Energy Resources Technology* 115 (4): 247-256. http://dx.doi.org/10.1115/1.2906429.

Wolf, S.F., Zacksenhouse, M. and Arian, A. 1985. Field Measurements of Downhole Drillstring Vibrations. SPE Annual Technical Conference and Exhibition Las Vegas, Nevada, 22-26 September. SPE-14330-MS. https://dx.doi.org/10.2118/14330-MS.

Appendix A

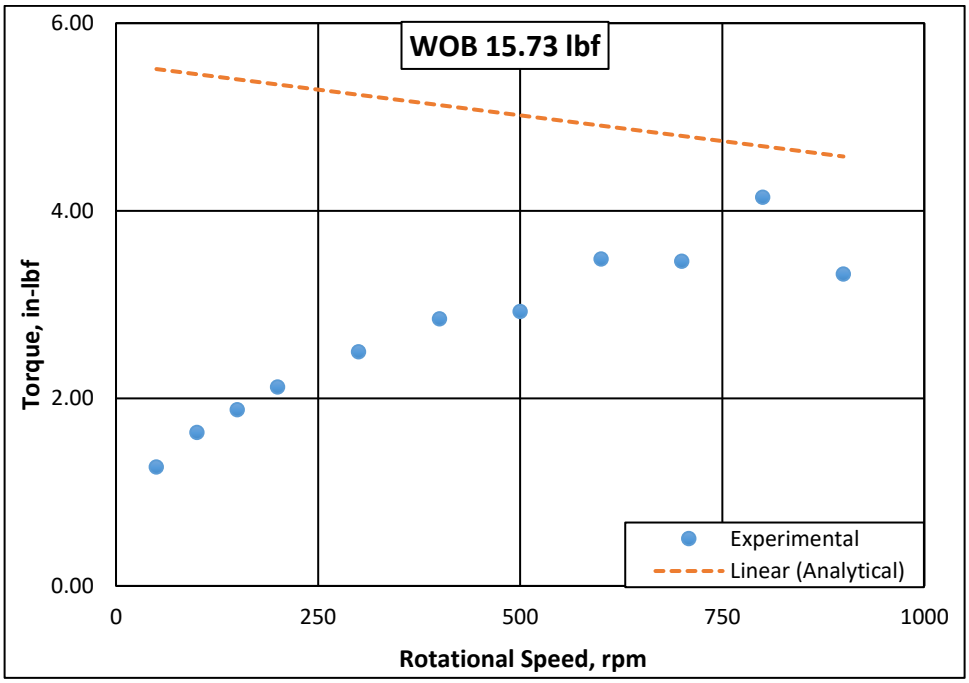

Figure A.1: Torque vs rotational speed at an average WOB of 15.73 lbf

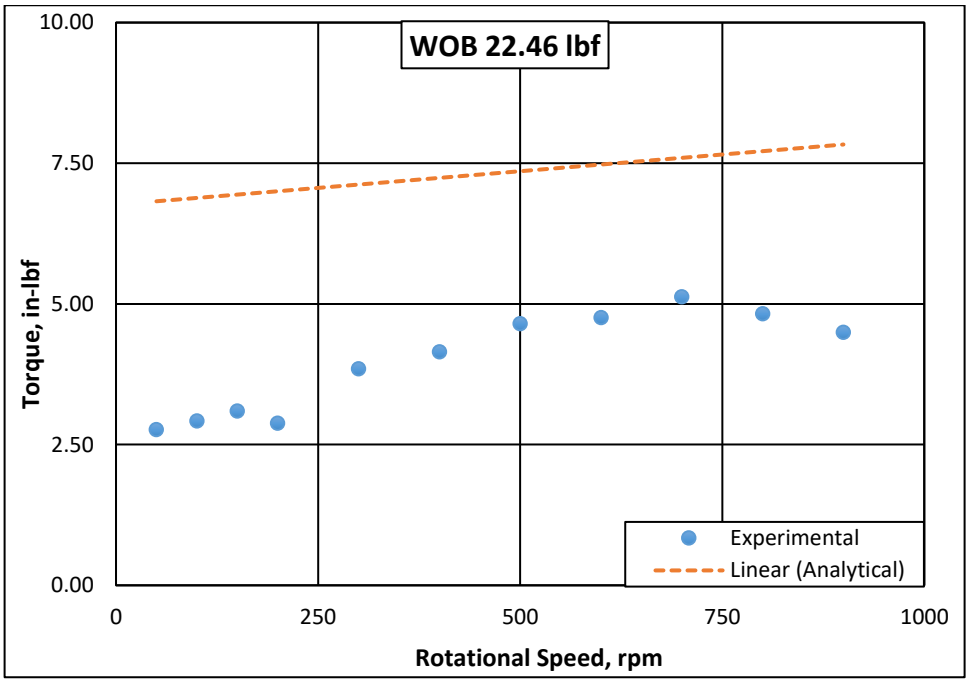

Figure A.2: Torque vs rotational speed at an average WOB of 22.46 lbf

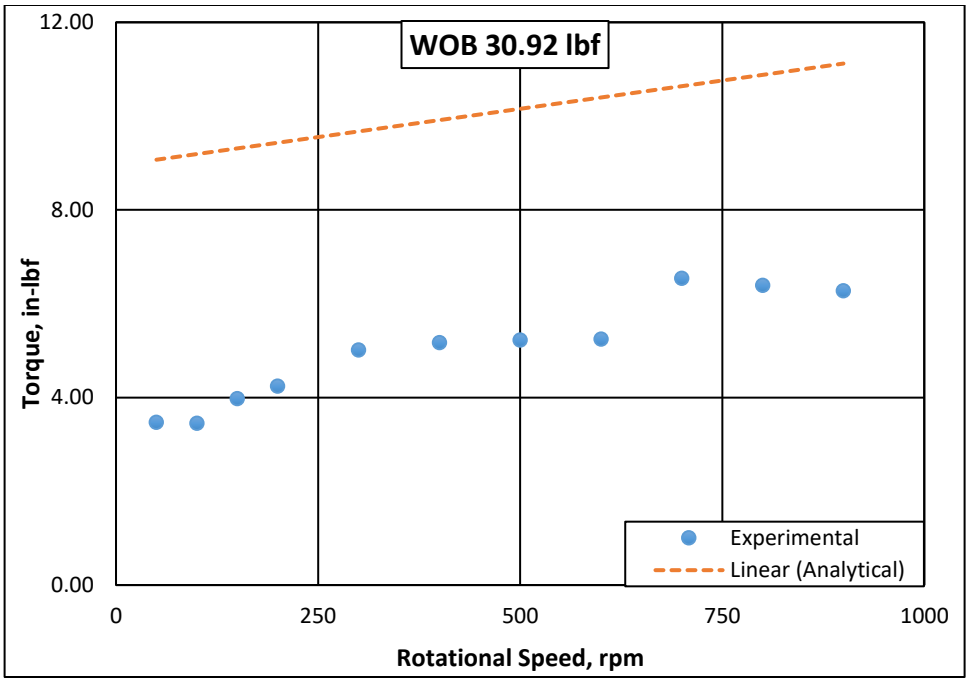

Figure A.3: Torque vs rotational speed at an average WOB of 30.92 lbf

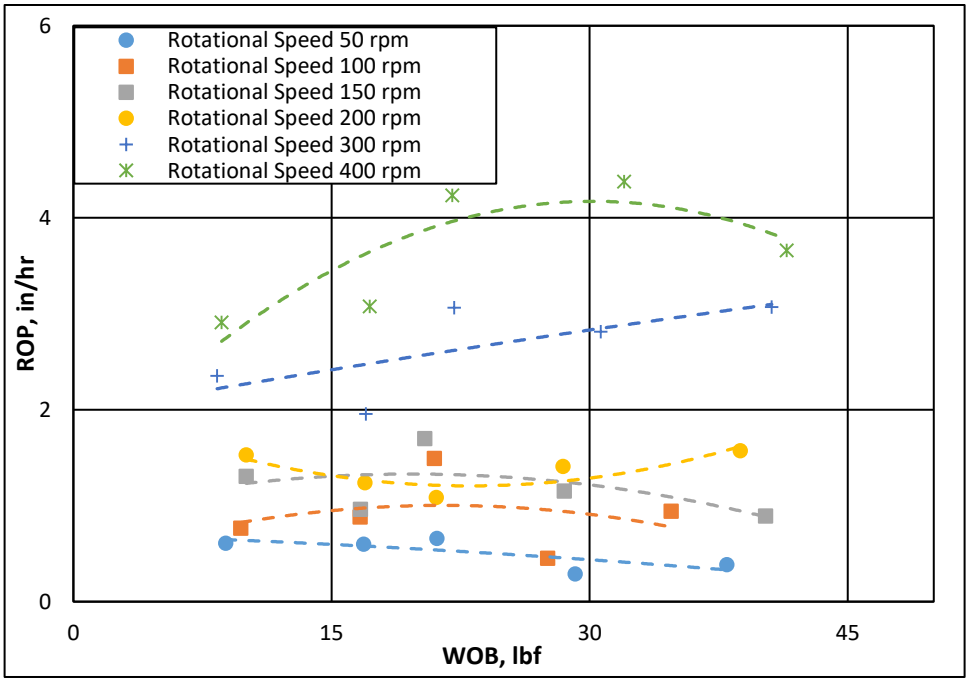

Figure A.4: ROP vs. WOB at constant rotational speed (soft sandstone)

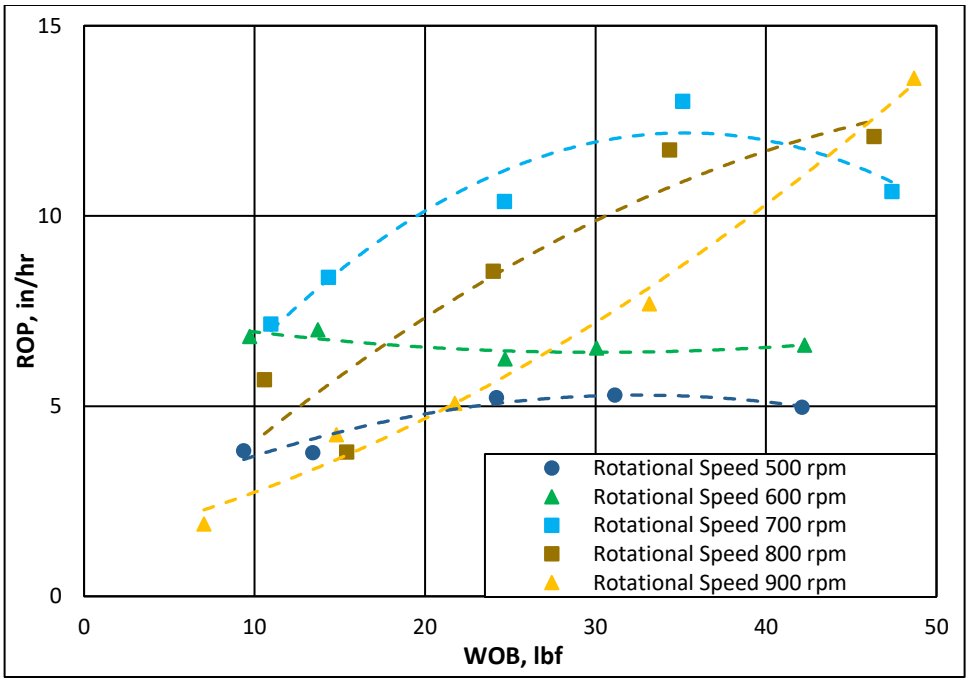

Figure A.5: ROP vs. WOB at constant rotational speed (soft sandstone)

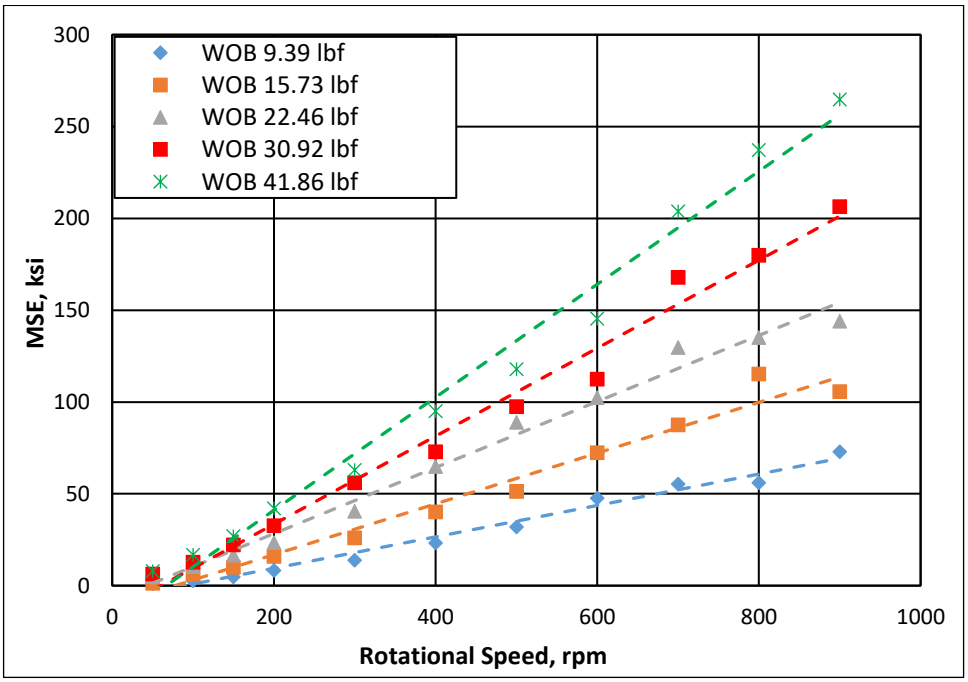

Figure A.6: MSE vs. rotational speed at constant WOB (soft sandstone)

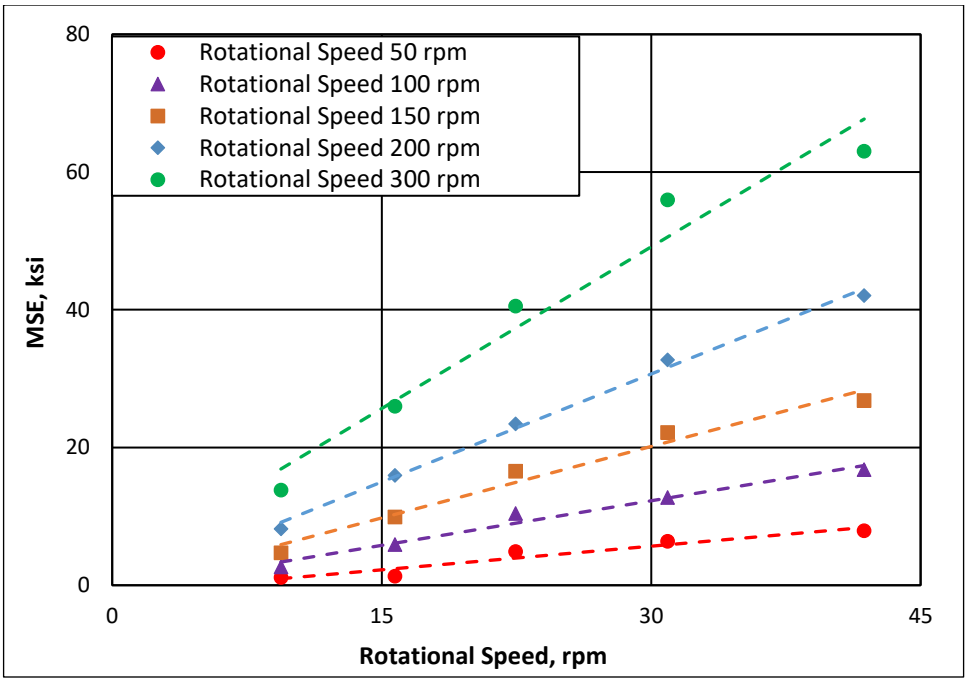

Figure A.7: MSE vs. WOB at constant rotational speed (soft sandstone)

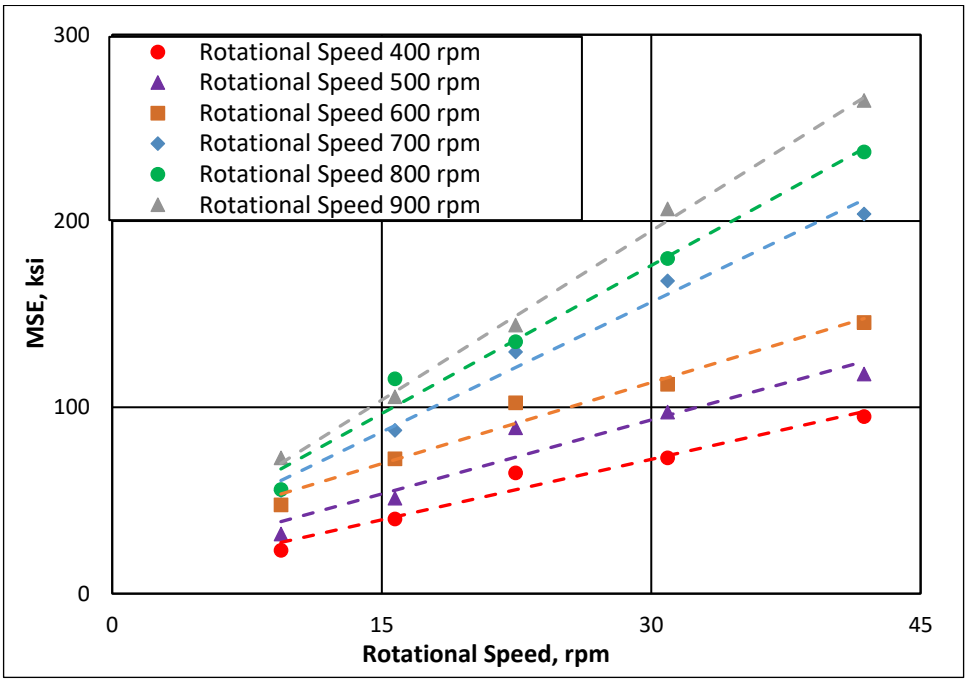

Figure A.8: MSE vs. WOB at constant rotational speed (soft sandstone)